PERIODICO di MINERALOGIA
established in 1930

DIPARTIMENTO DI SCIENZE DELLA TERRA
SAPIENZA UNIVERSITÀ DI ROMA

An International Journal of
Mineralogy, Crystallography, Geochemistry,
Ore Deposits, Petrology, Volcanology
and applied topics on Environment, Archaeometry and Cultural Heritage

Morphology, composition and source identification of urban aerosol particles in Vlora, Albania

Silvana Miço [1,*], Mirela Alushllari [2], Dode Prenga [1], Antoneta Deda [1]

[1] Department of Physics, Faculty of Natural Sciences, University of Tirana, Zogu I Boulevard, 25, Tirana, 1016, Albania
[2] Institute of Applied Nuclear Physics, Qesarake Street, 85, TIRANA, 1040, Albania

ARTICLE INFO

Submitted: February 2023
Accepted: June 2023
Available on line: September 2023

* Corresponding author:
silvana.mico@fshn.edu.al

Doi: 10.13133/2239-1002/18004

How to cite this article:
Miço S. et al. (2023)
Period. Mineral. 92, 261-285

ABSTRACT

This research aims to investigate the morphological characteristics, chemical composition and possible sources of aerosol particles. Aerosol samples of the urban atmosphere were examined in the city of Vlora, located in the south of Albania. Scanning electron microscope JEOL JSM-563 equipped with an Oxford Link ISIS L300 for energy-dispersive X-ray [EDS] analysis was used to examine aerosol particles. In addition, images of aerosol particles were processed by ImageJ software for dimensional and morphological analyses. The primary data automatically generated by ImageJ were surface, perimeter, minimal and maximal size, circularity, and aspect ratio parameters. Then, the projected area diameter, volume equivalent diameter (dev), physical diameter, and aerodynamic diameter were calculated. Based on the results of particle morphology and chemical composition nine groups of aerosol particles were classified: aluminosilicates (fly ash and soil particles), Ca-rich particles, carbon particles (soot particles and biogenic particles), sea salt particles, Si-rich particles, Fe -rich particles, and mixed particles. The morphological analysis results indicated that aerosol particles were relatively distributed over a wide size range of 0.5 μm to 28 μm fitted to lognormal distributions. In the measured distributions a peak around 2 μm is dominant. By accounting for volume equivalent and diameter aerodynamic shape factor, this study develops the method of the aerodynamic diameter calculation.

Keywords: Aerosol particles; SEM-EDS; Image processing; Morphology; Chemical composition; Distribution.

INTRODUCTION

Particulate matter, also known as aerosols, refers to non-gaseous materials that exist as distinct particles (liquid or solid) within the size range between few nm and tens of μm. These particles remain suspended in the atmosphere for significant periods of time. Depending on particle dimensions they remain suspended for long enough to penetrate the respiratory tract (Peters et al., 1997; Hinds, 1999; Taunton et al., 2011). Different epidemiological studies have documented that exposure to a high concentration of particulate matter is potentially associated with increased risks of respiratory and cardiovascular diseases (Heyder et al., 1986; Dockery et al., 1993; Pope et al., 1995; Bell and Davis, 2001; Piazzola et al., 2021). Airborne particles act as carriers of toxic substances, viruses, bacteria, and fungi, infiltrating the respiratory system. Consequently, exposure to particles of various shapes, sizes, and chemical compositions can have adverse effects on human health. The health impacts are contingent upon the physical and chemical properties of aerosol particles, and despite ongoing research, their exact role remains uncertain (West et al., 2016; Schraufnagel, 2020; Romano et al., 2020). Gaining a better understanding of the physical and chemical properties of airborne particles

can lead to an enhanced assessment of their impact on human health. All physical and chemical characteristics of particles are different due to the large variability of emission sources, formation, and post-formation mechanisms. Aerosol particles exhibit a wide range of sizes, shapes, chemical compositions, and natural or anthropogenic origin (WHO, 2006). Particle size described by a simple linear dimension or physical diameter can be uniquely defined only for spherical particles. However, for irregular-shaped particles, a specific parameter must be clearly defined to include not only physical dimension but also information on the density and shape (Isik and Cabalar, 2022). A well-known parameter called the equivalent diameter of irregularly shaped particles is defined as the diameter of a sphere that has the same value of physical property as that of the particle under consideration (Hinds, 1999). The equivalent diameter is determined by measuring a physical characteristic that is particle size dependent such as aerodynamic, inertial, diffusion, optical and electrical mobility (Baron and Willeke, 1993; Seinfeld, 1996). There are many aerosol size-measuring techniques based on these physical properties. The use of aerodynamic properties is widely accepted as more convenient (Hinds, 1999; Seinfield and Pandis, 1998; Tan, 2014) because these properties govern the mechanical processes affected by gravitational and inertial forces (transport, removal, deposition efficiency) and better describe the behaviour of particles into the air. The optical particle counters use the light-scattering phenomena described by Mie theory to calculate the spherical equivalent diameter of a particle (Nafiseh and Jason, 2019). Optical imaging techniques are used to measure the physical particle size based on analyzing the photomicrographs of the silhouette or projection of the particle (Lyman et al., 1990, Lu et al., 2007, Pachauri et al., 2013, Miço et al., 2019a, and Li et al., 2020). The inertial impactors classify particles into different sizes based on the particle's behaviour in the fluid flow field (Le and Tsai, 2021).

The routine monitoring of mass and number aerosol concentration is focused on the particle aerodynamic size distributions. The two most common modes of particles observed are the fine mode (particles with an aerodynamic diameter smaller than 2.5 μm, referred to as PM2.5) and the coarse mode (particles ranging between 2.5 μm and 10 μm, known as PM2.5-PM10).

Information about particle size, shape, and elemental composition is essential to understand the contribution of emission sources and the behaviour of aerosol particles into the atmosphere. These data cannot be taken from mass or number concentration distributions and chemical analysis only. Over the past to recent years, there has been an increased interest to address the problem of physicochemical characterization of aerosol particles by performing microscopy techniques (Ebert et al., 2002; Shandilya and Kumar, 2010; Sielicki et al., 2011; Cvetkovic et al., 2012; Miço et al., 2015, Zeb et al., 2018, Brostrøm et al., 2020, Li et al., 2020, Usman et al., 2022, and Mushtaq et al., 2022). Microscopy is considered as an absolute method to determine the size and shape of aerosol particles because it allows direct measurements and observations of individual particles (Baron and Willeke, 2001; Shen et al., 2007; Armiento et al., 2013; Bora et al., 2021). Although it is considered time-consuming to realize analyses of several particles statistically accepted, Scanning Electron Microscopy (SEM) coupled with energy dispersed X-ray analysis system (EDS) provides a powerful tool for the physicochemical characterization of aerosol particles (Post and Buseck, 1984). The usefulness of microscopic analysis of aerosol particles depends on the ability to convert measured sizes to other equivalent diameters that describe their behavior (Hinds, 1999; Brostrøm et al 2020; Miço et al., 2019a; Li et al., 2020). Combined with other measurement techniques it gives helpful information about the source and origin of aerosol particles.

In this article, the aerosol particle parameters evaluated by using SEM/EDX and image processing techniques are presented. It is also a report on the morphological characteristics of aerosol particles providing insights to understand their potential emission sources. The objective of this research is to employ microscopic techniques to investigate the physical and chemical properties of atmospheric aerosol particles and their potential sources. Given the diverse nature of airborne aerosols originating from various sources, a combination of different techniques is utilized. The Scanning Electron Microscope (SEM) technique is employed to provide photomicrographs and X-ray spectra of individual particles. Image processing techniques are applied to examine the morphological characteristics of individual particles. The study estimates particle size distribution, geometric and aerodynamic shape factors. Aerosol particles from different studied areas are categorized into distinct classes based on their chemical composition and morphological characteristics. Furthermore, this study develops a method to calculate the aerodynamic diameter, which differs from the physical or actual diameter due to variations in particle density and geometrical shapes, resulting in higher values. Alongside particle size, composition, and morphology, the dispersive effects of meteorological parameters and air masses that transport aerosol particles from different source regions are considered to identify the sources of particles.

PHYSICAL CHARACTERISTICS OF AEROSOL PARTICLES

Equivalent diameters

Projected area equivalent diameter, d_{pa}, is defined as the diameter of a sphere having the same surface area as

the projected area of particle silhouette (Olson, 2011). Equivalent diameter is given by:

$$d_{pa} = \sqrt{\frac{4S}{\pi}} \quad (1)$$

The surface approximated as the sum of each pixel within a *2-D* projected image can be converted by an image processing system in μm^2. Two other equivalent diameters also defined on the particles' silhouette, Martin diameter d_M and Ferret diameter d_F can be used in microscopic image analysis in addition to d_{pa} diameter (Hinds, 1999).

Volume equivalent diameter, d_{ve}, is defined as the diameter of a sphere having the same volume V_p as an irregular-shaped particle (Baron andWilleke, 1993), given by:

$$d_{ev} = \left(\frac{6V_p}{\pi}\right)^{\frac{1}{3}} \quad (2)$$

Shape factor

Geometrical shape factor, *R*, (roundness), is a dimensionless parameter characterizing the deviations of a particle shape from spherical ones and expressed in terms of surface and perimeter of particle silhouette *p* expressed as:

$$R = \frac{4\pi S}{p^2} \quad (3)$$

The maximum value of *R* is 1 for perfect spherical shapes and less than 1 for other particles, decreasing for more elongated geometrical shapes.

Volume shape factor, α_v, is another dimensionless parameter that relates particle volume V_p with projected area equivalent diameter of particle d_{pa} by:

$$\alpha_v = \frac{V_p}{d_{pa}^3} \quad (4)$$

Combining equations (2) and (4) gives

$$V_p = \alpha_v d_{pa}^3 = \frac{\pi}{6} d_{ev}^3$$

and volume equivalent diameter is given by:

$$d_{ev} = d_{pa}\left(\frac{6\alpha_v}{\pi}\right)^{\frac{1}{3}} \quad (5)$$

The value of α_v is 0.52 (or π/6) for a perfectly spherical particle and less than 0.52 for any other particle (Allen, 2003). The volume shape factor for all regular-shaped particles (cylindrical, cubic, prismatic) can be easily calculated simply using volume formulas, respectively. For irregular-shaped particles, the shape factor can be experimentally estimated by combining two or more methods (Hinds, 1999).

Wadell sphericity, ψ_s, is another shape factor determined as the ratio of the surface area of a sphere having the same volume as the particle under consideration to the particle surface area (Allen, 2003):

$$\psi_s = \frac{surface\ area\ of\ a\ sphere\ having\ the\ same\ volume\ as\ the\ particle}{particle\ surface\ area} \quad (6)$$

Wadell sphericity can be roughly found as the ratio of projected area equivalent diameter of particle silhouette to the diameter of the smallest circumscribing sphere X_{min} or Feret diameter (Masuda, 2012):

$$\psi_s \approx \frac{d_{pa}}{d_F} \quad (7)$$

Sphericity coefficient is 1 for perfect spherical shape and less than 1 for irregular-shaped particles.

Aspect Ratio, *AR*, is the ratio of the width to the height of the 2D particle projected image. *AR* can be expressed in terms of volume equivalent diameter and projected area equivalent diameter of particle (Ferrera et al., 1993) by:

$$AR = \left(\frac{d_{ev}}{d_{pa}}\right)^3 \quad (8)$$

Aerodynamic diameter

Stokes diameter, d_{ps}, is an aerodynamic particle size defined as the diameter of a sphere having the same terminal settling velocity and the same density as the particle in a fluid under the same conditions, corrected by Cunningham correction factor $C_c(d_{ps})$ based on this diameter. For a spherical particle at rest, the Stokes diameter is identical to the physical diameter of the particle: $d_p = d_{ps}$.

Aerodynamic diameter, d_a, is the diameter of a sphere with a standard density of 1 g/cm^3 having the same terminal settling velocity as the particle of interest, corrected by Cunningham correction factor $C_c(d_a)$ based on this diameter.

The relation between Stokes diameter d_{ps} and aerodynamic diameter d_a is given by Hinds, 1999:

$$d_a = d_{pa}\left[\frac{\rho_p C_c(d_{ps})}{\rho_0 C_c(d_a)}\right]^{\frac{1}{2}} \quad (9)$$

where ρ_p is the density of the particle under consideration and ρ_0 is the standard density (1 g/cm^3) of a sphere having the same inertial properties as this particle.

Cunningham correction factor (or slip correction factor) is an empirical factor that can be calculated by Hinds, 1999:

$$C_c = 1 + \frac{\lambda}{d_p}\left[2.34 + 1.05\exp\left(-0.39\frac{d_p}{\lambda}\right)\right] \quad (10)$$

where λ is the mean free path of the air molecules and is equal to 0.0673 μm at standard conditions (1 atm and 23 °C), calculated from the kinetic theory. For fine particles (less than 0.1 μm) as the size decreases slip correction factor increases and Equation 10 must be used. For particles with a diameter equal to or greater than 1 μm the expression of C_c factor is modified in the simple form:

$$C_c = 1 + \frac{0.157\mu m}{d(\mu m)_p}$$

The slip correction factor is usually neglected for particles greater than 10 μm in diameter.

The aerodynamic shape factor, χ, is defined as:

$$\chi = \frac{Drag\ force\ on\ the\ non\ spherical\ particle}{Drag\ force\ on\ the\ sphere\ of\ equivalent\ volume}$$

Wu and Colbeck (1996) have shown that the relation between aerodynamic shape factor and volume equivalent diameter is given by:

$$\chi = \left(\frac{d_{ev}}{d_{ps}}\right)^2 \quad (11)$$

In another way, Allen (2003) has shown the relation between the aerodynamic shape factor and sphericity factor expressed by:

$$\chi = \psi_s^{-1/2} \text{ or } \chi = \left(\frac{d_{pA}}{d_F}\right)^{-1/2} \quad (12)$$

The dynamic shape factor is equal to 1 for spherical particles and usually greater than 1 for any other particle. The dynamic shape factor increases as particle size increases (Reid et al., 2003; Kaaden et al., 2009).

MATERIALS AND METHODS

Study area

Aerosol particle samples were taken in an urban atmosphere in the city of Vlora, Albania. Vlora city, bounded by the sea and peninsula to the west and hilly terrain to the east, has a population of 117,850 residents according to the Census of Albania in 2011. The city covers a surface area of 1.6 km^2. The major anthropogenic sources of aerosol particles in Vlora city are related to traffic, waste combustion, unpaved roads, industrial wastelands, and construction without criteria. Figure 1 shows Vlora city map with six sampling points (Z1-Z6) accompanied by some images of the study sites indicating the buildings where the apparatus was placed. Samples were taken below the third floor of residential buildings. Sampling sites Z1, Z2, Z5, and Z6 are traffic-related areas and are considered urban sites throughout the study.

Urban site Z1: The Z1 site encompasses the area along the main boulevard of the city, which experiences high traffic density. Sampling was conducted for 7 days in August 2014 and 7 days in November to December 2014. The sampling point was situated on the second floor of a residential building adjacent to the boulevard.

Urban site Z2: The sampling site for Z2 was situated on the fourth floor of the Faculty of Technical Sciences, University of Vlora. This location, just a few meters from the sea, was chosen to represent a coastal area. The site is surrounded by large trees and a road with heavy traffic. Sampling was carried out for 3 days in July and 3 days in September 2014.

Suburban site Z3: Z3, classified as a suburban area, is situated in the outskirts of the city near the sea and a pine forest. Sampling took place for 3 days in August 2014 and 3 days in December 2014. The sampling point was surrounded by 1 to 3-story residential buildings and dense, large trees.

Background site Z4: Z4, located in the surrounding hills in Kanina at an elevation of approximately 350 m, is considered a background site. Sampling was conducted for 3 days in September 2014. The area in Kanina where the sampling took place is considered the background site.

Urban site Z5: Z5, classified as a suburban area, is located near the sea and a pine forest in the outskirts of the city. Sampling was performed for 3 days in August 2014 and 3 days in December 2014.

Urban site Z6: Sampling at Z6 was carried out for 6 days in January 2015 on the second floor of the pediatric hospital building. The hospital is situated on a road that connects the city with a large portion of rural areas.

Rural site Z7: Z7 is located approximately 12 km at coordinates 40.53685°N and 19.52983°E. The site is

Figure 1. Location of sampling site (Google map).

characterized by very few scattered houses and dense vegetation. Please note that rural site Z7 is not depicted in Figure 1.

Sampling

Filtration is the oldest and most widely used method for aerosol particle measurements. The transfer of aerosol particles into a compact sample enables the preparation of the sample for microscopic techniques (Baron and Willeke, 2001). To collect aerosol samples, an optical particle analyzer model GRIMM EDM 107 and an air pump Tipi Escort ELF were used at the 1.2 l/min and 3 l/min flow regimes, respectively. These devices measure according to EN12341, EN14907, and US-EPA standards. Aerosol particles were collected on polycarbonate filters with 37 mm diameter and PTFE filters with 47 mm diameter. Overloading the filters with particles would complicate particle analysis by electronic microscope. To overcome the problem of particle overloading the sampling time was selected to be 24 h based on preliminary tests to control particle density on the filter. 38 filter samples were collected for analysis. Filter samples were weighed before and after sampling time using a microbalance. Collected samples were put in plastic cassettes and stored until SEM/EDS analysis time in the laboratory at 25-30 ºC temperature and relative humidity under 50%.

The variations in aerosol particle emissions directly from vehicles or induced by vehicle-induced dust are influenced by daily traffic patterns. These variations may differ based on specific days of the week and individual routines but remain relatively consistent on a given road. The atmospheric particle emission factors are influenced by factors such as the vehicle type, traffic volume, speed, fuel quality, and road conditions.

In Figure 2, the daily variations of vehicles on the main boulevard of Vlora city are presented. The data was manually collected during a typical working day in June 2014, spanning two weeks from 6:00 a.m. to 10:00 p.m. Even the manually counting is affected by human error, the purpose was to collect data that describes the volumes and the types of vehicles. The analysis reveals that private diesel cars contribute significantly to the overall traffic flow. Throughout the day, there are several peaks observed in traffic volume. Notably, there are three peaks during the early morning hours at 8 a.m., 10 a.m., and 12 a.m., coinciding with the rush of people to institutions situated along the main boulevard, such as schools, coastline areas, seaports, the university, commercial centers, and tourist agencies. After noon, the traffic gradually decreases and then increases again at 4 p.m., reaching its maximum peak at 8 p.m., mainly driven by the flow towards the coastline. It is important to note that Vlora city does not have significant industrial activities, and most employment opportunities are in private businesses such as shops, bars, restaurants, and hotels along the coastline. During the months of July and August, there is a substantial increase in traffic flow due to the tourist season, while it remains relatively constant during other months, largely influenced by the city's routine.

The variability of meteorological factors, such as temperature, wind speed, and humidity, can lead to changes in atmospheric aerosols through processes

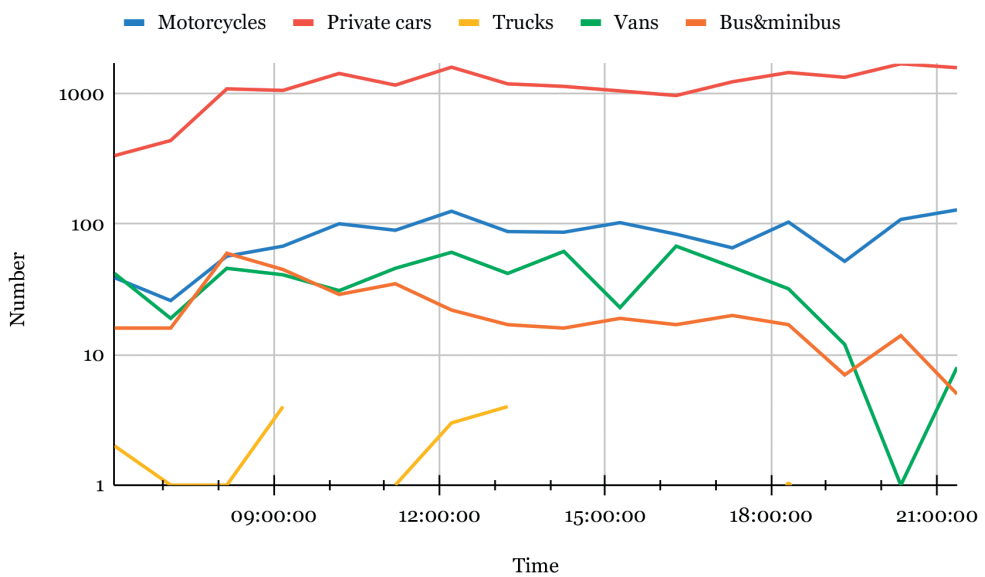

Figure 2. Daily variations of traffic in the main boulevard of the Vlora city during a common working day.

of accumulation or ventilation (Seo et al., 2018). Additionally, seasonal, and diurnal variations in wind direction can result in the transport of aerosol particles from different regions (Yang et al., 2020). Vlora experiences a typical Mediterranean climate characterized by warm to hot, dry summers and mild, wet winters. Hourly data on wind, temperature, and humidity were obtained from the meteorological station located on the terrace of the municipality in Vlora, measured at a height of 12 meters, using data provided by Meteoalb. Figures 3a and 3b show the commonly found wind roses for both sampling seasons. The average daily wind speed varies from 2-4 m/s. The average speed in summer was 2.2 m/s and in winter 2.6 m/s. Northeast winds predominate in the city of Vlora, in both the summer and winter seasons. There is a typical characteristic for coastal countries, during the day, westerly winds dominate, while at night hours, northeasterly winds prevail. During summer, the average relative humidity in Vlora is around 70%, while in winter, it increases to approximately 80%. Throughout the sampling periods, the average temperatures exhibit seasonal variations. In winter, the average temperature ranges from 11 ºC, with a minimum of -2 ºC in December, to a maximum of 26 ºC in November. On the other hand, summer temperatures range from a minimum of 15 ºC in June to a maximum of 35 ºC in August, with an average temperature of 27 ºC.

In addition, isobaric backward trajectories were calculated using the Hybrid Single-Particle Lagrangian Integrated Trajectory (HYSPLIT) model and the meteorological data of NOAA Air Resources Lab. website (http://www.arl.noaa.gov/ready/hysplit4.html). The calculation method of the NOAA HYSPLIT model is a hybridization between Lagrangian and Eulerian methods (Draxler and Rolpf, 2003). Five-day backward trajectories, during the sampling period, were calculated for 500 m, 1000 m, and 1500 m above the ground level ending at 06:00 UTC. Most common found backyard trajectories corresponding to the changing time of the collected filters are presented in Figure 4a and 4b.

Analysis of backward trajectories of air masses for specific days during the summer season shows that continental air masses coming from the region and continental sea air masses crossing the Adriatic from Italy or Croatia are dominant. Otherwise, during the winter season, the results show the dominance of long trajectories that start from the Mediterranean Sea and the Sahara Desert arriving in Vlora at low latitudes, smaller than 1000 m, where aerosol concentrations are commonly high. Many studies have shown that air masses from the Mediterranean Sea transport aerosols from different continental sources and are rich in Sahara dust (Papayanis et al., 2005; Querol et al., 2009; Dimitrou et al., 2022; Salvador et al., 2022).

SEM-EDS analysis

Qualitative analyses of individual aerosol particles were performed by using a scanning electron microscope (JEOL JSM-563 equipped with an Oxford Link ISIS L300 for energy-dispersive X-ray (EDS) analysis, located at the Department of Chemistry, University of Ioannina, Greece. SEM/EDS analyses were performed according to

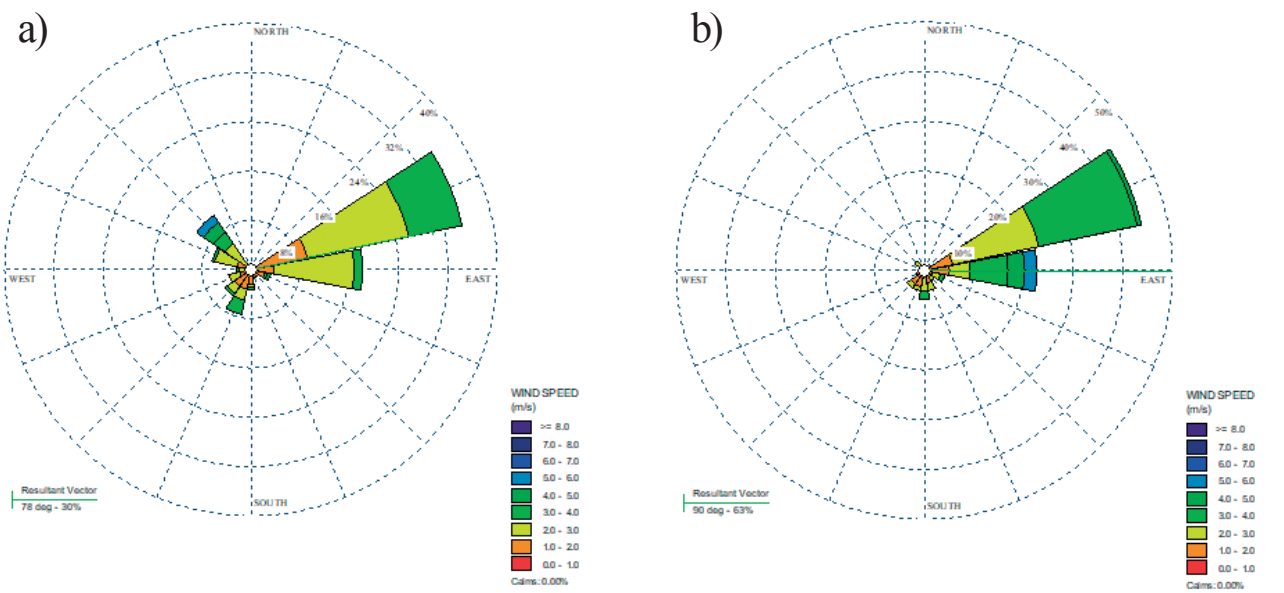

Figure 3. The most common wind roses for sampling periods in a) summer and b) winter in Vlora.

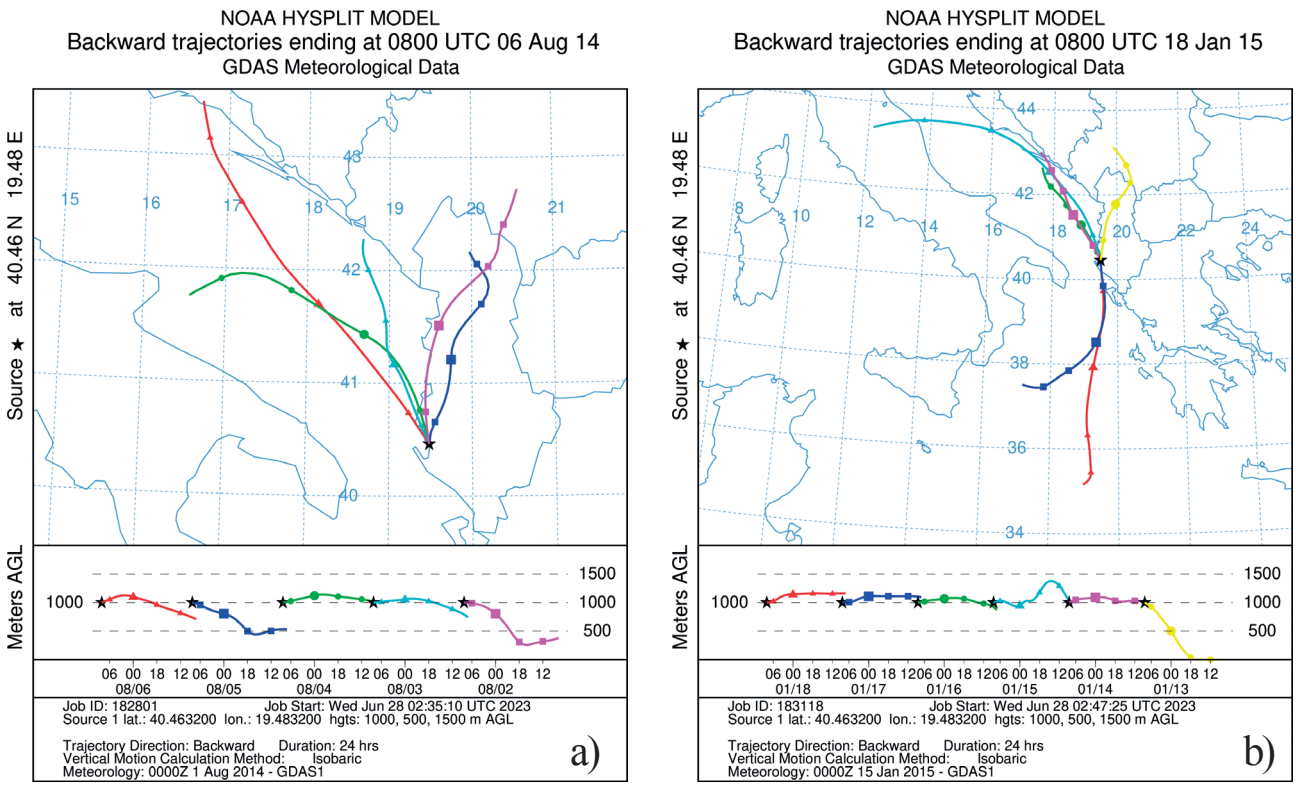

Figure 4. The most common five-day air-mass backward trajectories at 500, 1000 and 1500 m AGL latitudes, ending at 06:00 (UTC), for for the sampling periods in a) summer and b) winter in Vlora.

EPA Guidelines (2002). Correct preparation of samples for successful SEM analysis is of great importance and is related to the filter type used for sampling and the purpose of the study. Sections 5 mm by 5 mm of filters were cut from each sample and mounted with a carbon film on aluminum SEM stubs for analysis. The working conditions of accelerating voltage of 20 kV, probe current under 100 μA, and 21 mm working distance were set. To provide representative results and minimize subjectivity three randomly selected fields for each filter were examined and each of the particles within the field was analysed.

Manual SEM particle examinations were carried out at magnifications up to 8000 and secondary electron images were acquired. EDX spectra for the centre of particles on SE images with an energy range of 0-20 keV and a count rate of 5-33 cps with an approximate measuring time of 100 s were accumulated. Agglomerates with variable chemical composition present in PM samples were examined in different areas. Superfine particles, smaller than 0.5 μm, were not examined. To provide statistically significant results, about 100 particles per filter were analysed for their morphology. Photomicrographs of individual particles and selected fields and EDX data were saved for further examination. Chemical element analysis was performed for C, Ca, Al, Si, Cl, Na, K, P, S, Mg, Fe, Cr, Cd, Mn, Pb, Cu, Ti, Zn, Ni, Cs, and Co chemical elements. SEM images of aerosol particles were processed by ImageJ software for dimensional and morphological analyses.

Image processing

Since most of the analysed particles were irregularly shaped, the particle sizes are calculated based on the surface of the silhouette of the particles in the image. For the irregularly shaped particles, the usefulness of microscopic analysis lies in the possibility of converting measured dimensions into other equivalent diameters. SEM images of aerosol particles were processed by ImageJ software for dimensional and morphological analyses (Abramoff et al., 2004; Ferreira, 2003; Miço et al., 2019b). Uncertainties in the range of 0.5-1 μm are significant mainly for carbonaceous particles. After carefully setting the parameters, the software automatically generates the primary data such as surface, perimeter, minimal and maximal size, circularity, and aspect ratio. The physical parameters calculated by using the extracted data by the image analysis are the projected

area diameter of particles (d_{pa}), the volume equivalent diameter (d_{ev}), Stokes diameter (d_{ps}), and aerodynamic diameter (d_a) (Olson, 2011).

Using these morphological characteristics of particles and their chemical composition by X-ray spectra, equivalent diameters of aerosol particles can be easily calculated.

RESULTS AND DISCUSSIONS

Physical and chemical characteristics of aerosol particles

After the parameters have been carefully set, the ImageJ software automatically generates the primary data such as surface, perimeter, minimal and maximal size, circularity, and aspect ratio. The physical parameters calculated by using the data attained by the image analysis are the projected area diameter of particles (d_{pa}), geometrical shape factor (R), Wadell sphericity (ψ_s), Cunningham correction factor $C_c(d_{ps})$, aerodynamic shape factor (χ) and the volume equivalent diameter (d_{ev}) [6].

Once these parameters and particle density are known the particle's physical diameter and aerodynamic diameter are calculated. The density values of individual particles were used according to aerosol particle classification (Horvath, 1998; Sokolik and Toon, 1999; Barthelmy, 2006, Tegen et al., 1999).

Stokes diameter and aerodynamic diameter are calculated using equations (9) and (11).

Since ρ_0 is the standard density of 1 g/cm^3, equation (9) can be written in the form:

$$d_a\sqrt{C_c(d_a)} = d_{ps}\sqrt{\rho_p C_c(d_{ps})} \tag{13}$$

For non-very small particles (at standard conditions (1 atm and 23 °C) and mean free path of 0.0673 μm) aerodynamic diameter is related to physical diameter by:

$$d_a\sqrt{1+\frac{0.157}{d_a}} = d_{ps}\sqrt{\rho_p\left(1+\frac{0.157}{d_{ps}}\right)} \tag{14}$$

If the particle density and physical diameter (d_{ps}) are known, the aerodynamic diameter of a particle by solving equation (14) is found. The physical diameter (d_{ps}) and aerodynamic diameter (d_a) are calculated using the volume equivalent diameter, the particle density, and aerodynamic shape factors.

Figure 5 shows examples of SEM images for particles with different morphology, size, and chemical composition. Figure 6 shows respective EDX spectra of particles shown in Figure 5. In Figure 6, the spectra corresponding to particles c, d, k, and p are not presented. The spectra

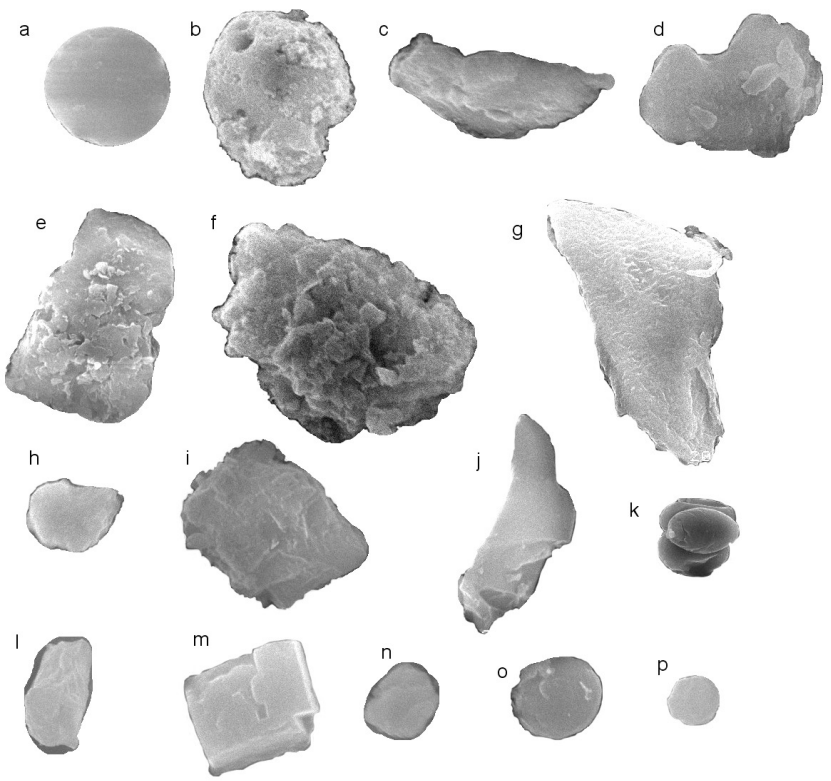

Figure 5. Examples of particles with different morphology, size and chemical composition.

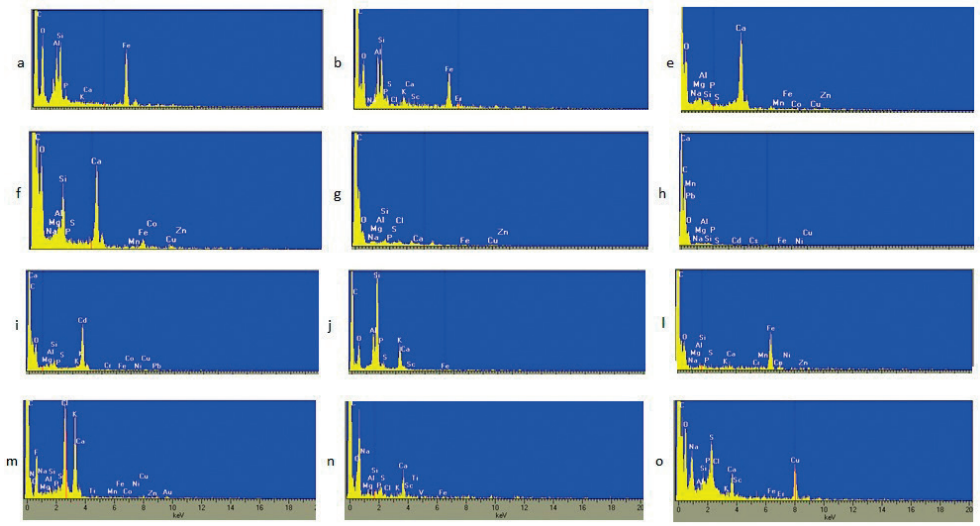

Figure 6. EDX spectra of particles shown in Figure 5.

of particles c and d were similar to that of particle b, indicating that they are classified as aluminosilicate (Al-Si) soil particles. Particle k exhibited a spectrum similar to particle g, suggesting that both particles are carbon-rich and classified as biogenic particles. The distinctive morphologies of these particles were sufficient for their classification.

The spectrum of particle p resembled that of particle e, both being rich in calcium (Ca). Although their shapes and sizes significantly differ, their chemical composition is the same. This indicates that the mechanisms of their formation or the subsequent processes after formation were different. This highlights the advantage of the scanning microscopic method compared to other chemical or physical methods, as it provides valuable insights into the differences in particle formation and processes.

Examination of the photomicrographs results in a variety of shapes, mostly irregularly shaped with sharp edges that cause their optical properties to differ significantly from those calculated through the Mie theory which considers spherical particles.

The study of particle morphology is important not only for the assessment of their optical properties but also because it affects the process of their deposition in the respiratory system. Morphology and chemical composition are crucial factors in identifying the sources of atmospheric aerosols (Usman et al., 2022).

Average particle density values for aerosol individual particles classified into different groups (Ebert, 2002; Tegen and Fung, 1994;) are presented in Table 1. The numerical

Table 1. Average particle density of aerosol individual particles classified in different groups (Ebert M., 2002; Tegen and Fung, 1994).

Particle Groups	Elemental composition	Density (g cm^{-3})
Silicates	Al+Si>60%	2.6
Carbonates (calcites, dolomites)	Ca>60% and S<20% Al, Si, Mg, and K content	2.7
Soot aggregates	C content higher than O	1.0
Biogenic particles	C and O in the same amounts and Na, P, Cl and S contents	1.3
Metal oxides	Al, Ti, Mn, Fe, Cu, Ni, Zn, Cd or Pb>80%	4.5
Quartz (SiO_2)	Si dominant variable amounts of Al, Na, Mg.	2.6
Sea salt particles	Cl and Na with content of K, Ca, Mg and Si	2.2
Mixed particles	Variable combination of Ca, Si, Al, Mn, Cd, Pb, Mg and Fe with trace of P, S, Na, Cu, Co and Ni	2.5

values of physical parameters (surface, perimeter, Ferret's diameter, roundness, and aspect ratio) calculated automatically by using Image J software are presented in Table 2. The shape factors and equivalent diameters (projected area equivalent diameter, volume equivalent diameter, Stokes diameter, and aerodynamic diameter) calculated for the particles shown in Figure 5 are also summarized in Table 2. Particle density values according to the aerosol particle classification from Table 1 were used.

Probability distribution functions

Probability distribution functions (PDFs) and cumulative distribution functions (CDFs) are fundamental concepts in statistics and are closely related. The CDF represents the cumulative values of the PDF, and the PDF is simply the derivative of the CDF. To mitigate the sensitivity to binning, the PDFs were estimated using the method of linear least-squares fit of the CDFs. The optimization process was carried out using MATLAB programming.

To approximate and describe the parameter distributions, probability density functions were fitted to the calculated data. The integration of PDFs with respect to a given parameter over its entire range yields a result of unity. Lognormal size distributions are commonly observed to be the best fit for aerosols originating from a single source. Dunbar and Hickey (2000) estimated the application of probability density functions (PDFs) and curve fitting methods to approximate particle size distributions emitted from four single sources. They showed that no single probability density function represented the particle size distributions. Shen et al. (2020) verified whether other functions can describe atmospheric aerosols distribution. Furthermore, Anderson (2021) provides an explanation of the physico-chemical mechanisms that influence aerosol distributions in the environment, such as the mixing of different sources.

In the present study, 17 theoretical distributions were initially examined for the five aerosol components (d_{pa}, d_a, *R, AR* and χ), and based on goodness-of-fit tests, the 3 best-fit distributions were selected. Table 3 displays the values of two characteristic parameters, the mean value and standard deviation (σ), for the five calculated aerosol components.

Projected area diameter

The study of particle size distributions is crucial for understanding the mechanisms involved in particle formation and subsequent processes. In this study, individually identifiable particles were counted and measured in randomly selected fields of filters. Soot aggregates and tightly bound agglomerates were treated as individual particles, and their surface equivalent diameter

Table 2. Summary of morphological characteristics of aerosol particles presented in the Figure 5.

Nr.	A (μm^2)	p (μm)	d_F (μm)	R	AR	Elem. compos dominant	ρ gcm^{-3}	d_{pa} (μm)	d_{ev} (μm)	χ	d_{ps} (μm)	d_a (μm)
a	22.1	17.5	5.470	0.98	1.05	Si, Al, Fe	2.6	5.31	5.40	1.01	5.36	8.4
b	37.2	25.9	7.830	0.83	1.20	Si, Al, Fe	2.6	6.88	7.31	1.07	7.08	10.1
c	28.7	32.6	10.590	0.37	2.70	Si, Al, Fe	2.6	6.05	8.42	1.32	7.32	6.1
d	46.4	29.2	9.620	0.69	1.48	Si, Al, Fe	2.6	7.69	8.76	1.12	8.28	10.3
e	60.7	34.2	10.990	0.65	1.61	Ca	2.7	8.79	10.31	1.12	9.75	11.7
f	63.6	33.9	11.030	0.72	1.39	Ca, Si, Al	2.7	9.00	10.05	1.11	9.55	12.6
g	16.8	28.5	7.541	0.43	1.70	C (bio.frag.)	1.3	4.63	5.52	1.28	4.89	3.9
h	12.9	14.0	4.908	0.83	1.32	Ca, Mn, Pb	2.7	4.05	4.45	1.10	4.24	5.8
i	16.3	16.9	5.572	0.68	1.35	Ca, Cd	2.7	4.56	5.04	1.11	4.79	6.4
j	28.2	25.9	10.260	0.53	2.49	Si	2.6	5.99	8.12	1.31	7.10	6.2
k	201.9	54.5	19.740	0.86	1.49	C (spore)	1.3	16.04	18.32	1.11	17.39	15.2
l	13.2	14.8	5.571	0.76	1.88	Fe	4.5	4.10	5.06	1.17	4.69	5.1
m	19.2	17.4	5.956	0.80	1.24	Cl, Na	2.2	4.95	5.32	1.10	5.08	6.5
n	3.5	7.1	2.358	0.88	1.20	Na, Cl, P, Ca	2.2	2.12	2.25	1.05	2.19	2.9
o	13.4	13.6	4.263	0.97	1.05	Cu, C	4.5	4.13	4.20	1.02	4.17	6.4
p	1.7	4.8	1.527	0.96	1.04	Al, Mg, Si, Ca	2.5	1.46	1.47	1.02	1.45	2.2

Table 3. Mean values and standard deviations for the five calculated aerosol components.

Aerosol Component	PDFs parameters			
	Summer		Winter	
	Mean value	Standard deviation (σ)	Mean value	Standard deviation (σ)
Physical diameter d_{pa} (µm)	3.0275	3.0275	2.6497	2.2071
Aspect ratio	1.6441	1.6441	1.6203	0.4570
Roundness R	0.7695	0.7695	0.7184	0.1815
Aerodynamic shape factor χ	1.1588	1.1588	1.2034	0.1780
Aerodynamic diameter d_a (µm)	5.5851	5.5851	5.0835	4.1088

was calculated. It should be noted that the method used in this study is limited to particles larger than 0.5 µm due to the resolution limitations of the scanning microscope used for measurements.

For each filter, approximately 100 particles ranging in size from 0.5 to 28 µm were analysed. Figure 7a and 7b display the particle size probability distributions for 875 and 742 aerosol particles collected in urban area Z1 during the summer and winter periods, respectively. The x-axis represents the size scale in micrometers corresponding to the projected area diameters (d_{pa}) and the y-axis represents the number of particles and the corresponding probabilities of occurrence within the size ranges.

It was consistently found that the Inverse Gaussian (IGD), Generalized Extreme Values (GEVD), and Lognormal (LOGD) distributions were 3 best fits for particle size in summer and winter season.

From the plots, it is evident that the broadest distributions occur with the smallest particle sizes, and the width of the distribution decreases as the particle size increases. The distribution functions of d_{pa} yielded a mean value of 3.0275 and standard deviation of 3.0808 in summer and the mean value of 2.6497 and standard deviation of 2.2071 in the winter. The large standard deviation indicates a high degree of dispersion of the data relative to the mean. The median value of both PDFs was found to be 1.857 µm and 1.861 µm.

Aerosol particles in the size range of 0-2 µm accounted for 58% in the summer period compared to 68% in the winter period. The statistical parameters presented in Table 4 support this observation. The particle size distribution is dominated by the smallest particles, with 93% (in summer) and 95% (in winter) of particles having diameters less than 6 µm. The PDFs indicate that particles larger than 10 µm have a lower probability of being present in the atmosphere, reflecting the processes that remove aerosols from the atmosphere. These particles contributed approximately 3.4% of the total particles in the summer period, compared to 1.3% in the winter period, highlighting the diffusion and dispersion processes that control aerosol transport.

Aerosol particle morphology

The PDFs of the morphological parameters of aerosol particles examined are roundness , aspect ratio and aerodynamic shape factor χ. Due to a high amount of irregularities, aerosol aggregates are excluded from the calculation of these parameters in this study. Calculating

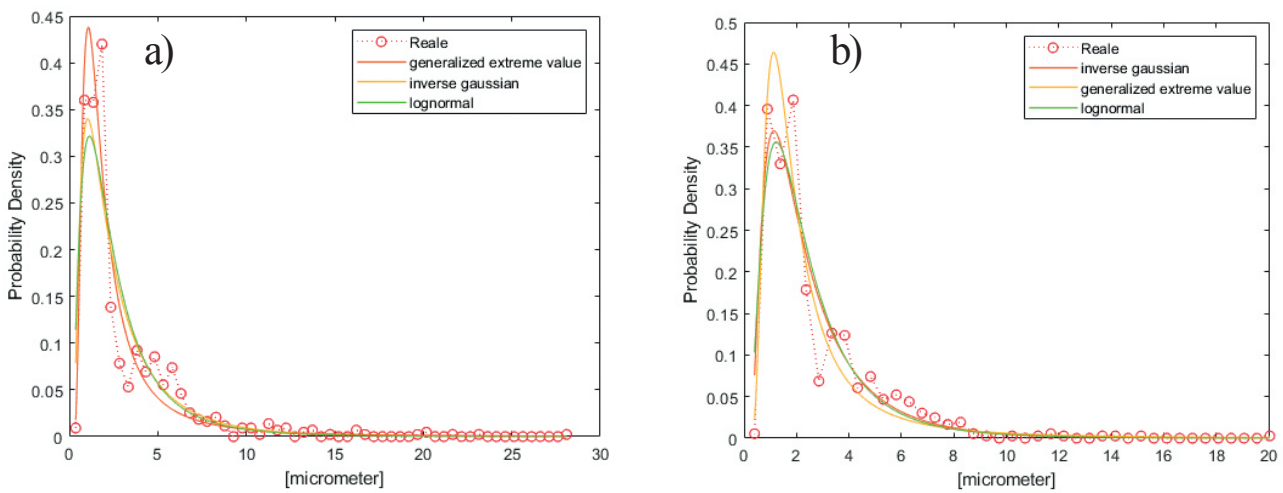

Figure 7. Probability distribution functions (PDFs) of physical particle size during a) summer and b) winter season.

Table 4. Classification of aerosol particles and relative abundance of different groups.

Groups	Sub-groups	Chemical composition	Morph.	Size (μm)	Abudance (%)									
					Summer				Winter					
					Z1	Z2	Z3	Z4	Z1	Z2	Z3	Z5	Z6	Z7
					875	289	295	291	742	286	275	308	530	227
Alumino -silicates	Si- Al-/fly ash	Si, Al dominant, moderate amounts of Fe and Ca with Na, Mg, Cr, S, and P content	Spherical	0.5-5	14.4	14.0	12.5	4.5	16.6	11.8	8.0	10.7	17.4	6.2
	Si- Al-/soil		Irregular	0.5-30	16.6	16.4	19.0	18.9	20.4	22.5	23.3	24.0	17.7	18.9
Ca-rich	Kalcite ($CaCO_3$)	Ca dominant with amounts Al, Si, Mg, S and K	Irregular	0.5-30	17.8	19.2	16.3	24.7	22.6	23.2	19.0	25.0	21.7	33.5
Soot	C-O	C content higher than O	Aggregate	0.5-4	13.3	11.2	7.5	4.1	18.1	12.5	10.9	12.3	19.4	7.5
Biogenic	C-O	C and O in the same amounts and N, P, Cl and S contents	Typical	1-20	9.0	10.1	12.2	12.0	2.7	4.8	9.0	5.8	3.8	11.9
Si-rich	Si-O	Si dominant variable amounts of Al, Na, Mg and trace of S, K and Ca	Irregular	1-10	4.0	5.8	5.1	7.2	2.6	5.9	9.4	5.5	4.0	5.3
Fe-rich	Fe-0	Fe dominant with traces of Na, Mg, Al, Si, k, Ca, Cr, Mn, Co and Zn.	Irregular	1-10	3.4	5.2	2.4	5.1	2.6	5.2	3.4	3.2	2.5	2.6
Sea salt	Fresh+aged	Cl and Na with content of K, Ca, Mg and Si	Crystal or rounded	1-5	17.3	17.8	19.7	17.2	9.7	8.6	11.0	7.1	8.1	5.3
Mixed	Variable components	Variable combination of Ca, Si, Al, Mn, Cd	Irregular or rounded	0.5-10	4.2	3.2	5.4	6.3	4.9	5.5	4.0	6.2	5.5	8.8

the shape parameters and aerodynamic diameter of particle aggregates requires detailed knowledge of the particle morphology. Depending on the time of their formation aerosol aggregates can vary from chain-like agglomerated shapes to compact structures. Mandelbrot's fractal formalism can be used to describe the particle morphology (Dhoqina et al., 2019). Hence, PDFs of particle shape factors are graphed for 759 and 608 aerosol particles collected in the urban area Z1 in the summer and winter periods, respectively.

Roundness

The geometrical shape factor *R* is important to evaluate the sharpening of particles. Figure 8 shows typical particles classified according to their geometrical forms where the numbers in brackets represent roundness . Particles are classified based on the roundness *R* calculated by equation (3).

Particle shape PDFs obtained by image analyses of total samples collected during the summer and winter periods in urban zone Z1 are shown in Figure 9a and 9b.

The Generalized Extreme Value Distribution (GEVD), Extreme Value and Weibull functions resulted the best fits when describing the aerosol distribution as a function of the roundness shape factor in summer and winter season. Broadest distributions occur with rondness in the range 0.7-0.9. The distribution function of *R* gave the mean value of 0. 7695 and standard deviation of 0.1723 in summer and on the other hand the mean value of 0.7184 and standard deviation of 0.1815 in winter season.

Roundness values *R* varied from 0.2 for more elongated particles to 1 for spherical particles. Particle shape factor

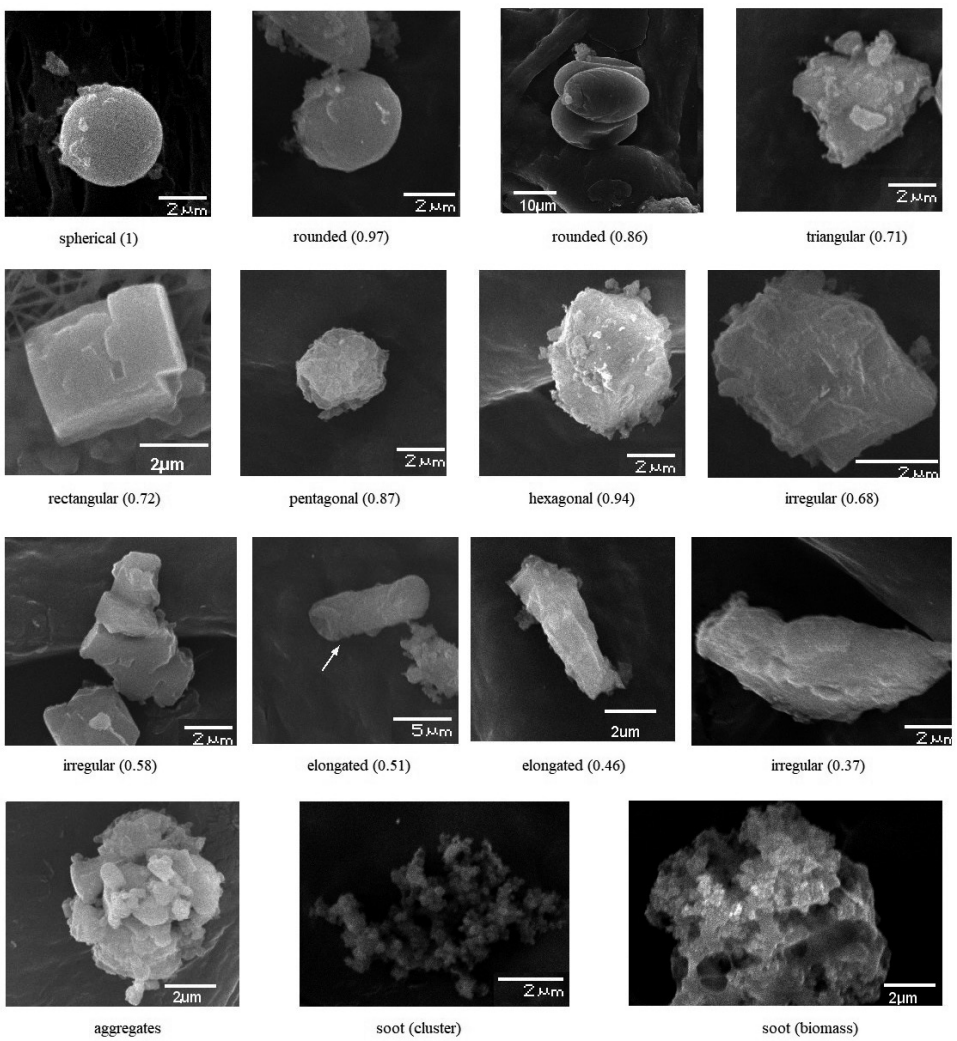

Figure 8. Photomicrographs of particles with different geometrical shapes (values in brackets represent corresponding roundness R).

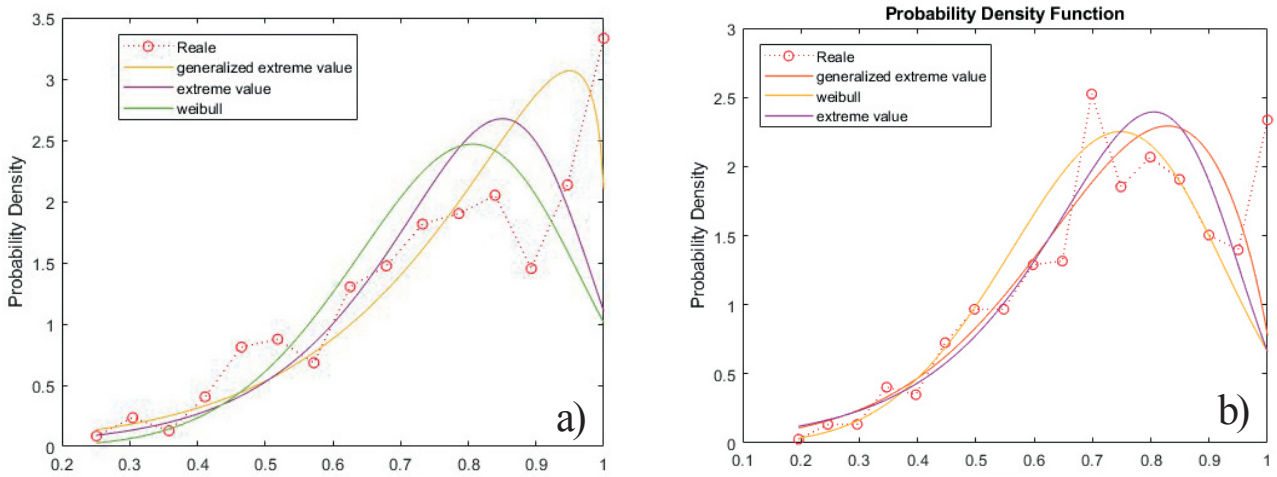

Figure 9. Probability distribution functions (PDFs) of particle roundness shape factor during a) summer and b) winter season.

in the size range 0.5-0.97 amount to 84% in summer compared to 78.8% in the winter period. This suggest that most particles are neither spherical nor very irregular. Urban atmosphere in winter have more very irregular particles than in summer period (5.2% vs 3.5%). Rounded to perfect spherical particles were found in similar percentage (1.7%, 1.5%). This implies strong interactions among meteorology and physical and chemical processes that undergone aerosol particles in atmosphere since their emission to the deposition onto the collection surface. Based on their geometrical shape, particles can be classified into different categories:

Elongated and very irregular particles: These particles have a shape factor ranging from 0.3 to 0.5. They exhibit elongated and highly irregular shapes.

Irregular particles: This category includes particles with a shape factor ranging from 0.5 to 0.7. They have irregular shapes but are less elongated compared to the previous category.

Regular triangular particles and rectangular particles: Particles in this category have a shape factor ranging from 0.7 to 0.8. They possess regular triangular or rectangular shapes.

Pentagonal, hexagonal, octagonal to decagonal particles, and ellipsoidal particles: These particles have a shape factor ranging from 0.8 to 0.97. They exhibit shapes with multiple sides, such as pentagons, hexagons, octagons, decagons, or ellipsoids.

Rounded and not perfectly spherical particles: This category includes particles with a shape factor ranging from 0.97 to 0.99. They have rounded shapes but may not be perfectly spherical.

Perfectly spherical particles: These particles have a shape factor of 1, indicating a perfect spherical shape.

By categorizing particles based on their geometrical shape, researchers can gain insights into their physical characteristics and potential sources.

The average value of the shape factor value of analysed particles is 0.78 with a standard deviation of 0.14. The angular and irregular-shaped particles dominate over the total particles. These particles came up from 60 to 70% of the total particles analysed. Our results agree with Carabali et al. (2012), Mogo et al. (2005) and Tian et al. (2019) indicating the influence of physical and chemical processes on the particle shape. Aglomerates were classified as a separate group, regardless of their shape and without calculating their geometrical shape factor, due to the high amount of sharpening. They constitute about 20% of total particles. The formation of aggregates comes from the clustering of primary spherical particles or smaller irregular particles depending on their origin. Aggregates of spherical individual particles smaller than 0.5 μm are derived by combustion processes at high temperatures and are known as soot aggregates (Kandler et al., 2009, Carabali et al., 2012, Bhandari et al., 2019). They constitute the main part of aggregates of about 95%. Aggregates of irregular particles, which are of mineral or soil origin, are compact and make up less than 5% of all aggregates. Rounded and spherical particles having shape factor values of great than 0.95 predominated the fine particle fraction. Spherical particle number of a coarse fraction having physical diameter values of great than 2 μm is very small. Being mostly with Fe content, these particles are assumed to be attributed aerosols of anthropogenic origin. The 1-2 μm intermediate fraction and the coarse fraction were dominated by regular angular (triangular and square) particles likewise irregular particles in agreement with results of Okada et al. (2001).

Aspect Ratio

The aspect ratio (*AR*) of particles is another factor that plays a role in particle deposition processes. Figures 10a and 10b display the aspect ratio density functions for urban zone Z1 during the summer and winter seasons. The IGD, GEVD and Bimbaumsaunders functions provide better fits to the data for describing the aspect ratio aerosols in both summer and winter season. The mean aspect ratio values were calculated as 1.6441 in the summer and 1.6203 in the winter season. These values are consistent with those reported by Komar et al. (2022). The standard deviation of aspect ratio, which reflects the degree of dispersion of data relative to the mean, is 0.5407 in the summer season and 0.4570 in the winter season.

Komar (2022) argued that the aspect ratio of particles is influenced not only by primary and secondary processes such as production, transportation, and aggregation but also by meteorological conditions, particularly humidity. For particles composed of water-soluble elements, the aspect ratio tends to approach unity upon humidification. However, it is important to note that the treatment of samples examined by SEM may lead to an overestimation of particle aspect ratio.

By studying the aspect ratio of particles, researchers can gain insights into their shape characteristics and how they may interact with the environment and undergo transformation processes.

AR values determine the length/width ratio, and the same value can be obtained both for large particles and small ones when length changes are associated with the same width changes. Hence, *AR* values are not significantly different for most of the particles. The *AR* ratio is not very different for most particles with roundness from 0.7 to 1 which belong to the angular and spherical particles. Otherwise, for elongated particles, *AR* ratio varies significantly. *AR* ratio is not only greater but also significantly different for elongated particles with less than 0.5. Other studies have demonstrated that the aspect ratio does not depend on particle size (Okada et al., 2001; Kandler et al., 2011). Different shapes of particles depend on the physicochemical processes during and after their formation.

Aerodynamic shape factor

Differently from the two factors *R* and *AR* measured directly from the SEM micrographs, the aerodynamic shape factor χ was calculated by using equation (11). It is an empirical assessment based on experimental data. The probability density functions of the aerodynamic shape factor for both summer and winter season in Z1 area is determinded as shown in Figure 11a and 11b. The aerodynamic shape factor varied from 1 for spherical particles, 1.04 for square particles to 1.94 for elongated particles with distinctive aerodynamic shapes like the c and m particles in Figure 5. The GEVD, loglogistic and LOGD resulted the best fit functions for describing aerodynamic shape factor.

The density functions of χ yield a mean value of 1.1588 and a standard deviation of 0.1464 in the summer season, which are slightly smaller than the mean value of 1.2034 and standard deviation of 0.1780 in the winter season. These values indicate the central tendency and dispersion of the aerodynamic shape factor distribution for aerosol particles in each season.

The aerodynamic shape factor plays a role in determining the settling velocity and deposition behavior of particles in the atmosphere. By studying the distribution of this parameter, researchers can gain insights into the aerodynamic properties of aerosols and their potential sources, as well as the processes

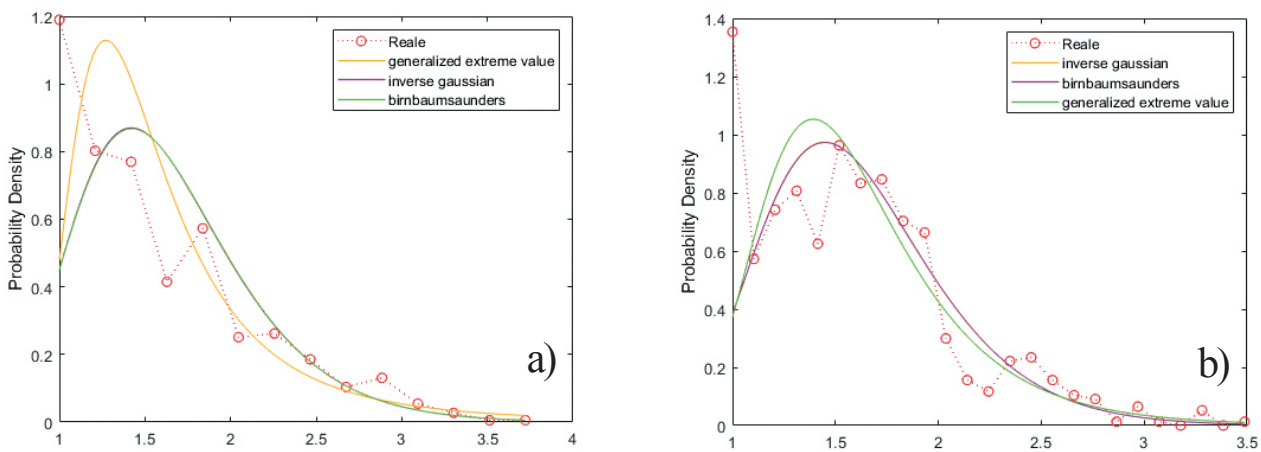

Figure 10. Probability distribution functions (PDFs) of aspect ratio during a) summer and b) winter season.

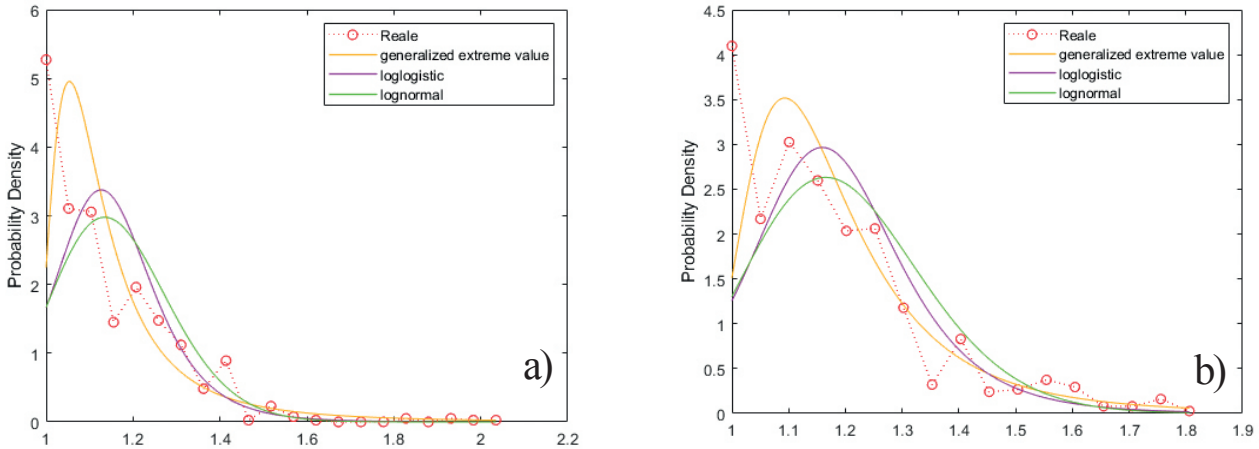

Figure 11. Probability distribution functions (PDFs) of aerodynamic shape factor during summer season.

that influence their transport and removal. Angular and elongated particles are more hazardous to human health than rounded particles because, being edge-sharped, have greater aerodynamic factors and can deeper penetrate the respiratory system (Hassan and Lau, 2009). These particles are mainly formed by mechanical processes such as breaking and crushing. But they also can be formed by chemical reaction between sulfur compounds and other particles, by chemical reactions among pre-existing solid, liquid or gaseous phases, or by aggregation of pre-existing particles (Bora et al., 2021).

Classical aerodynamic diameter

The Probability Density Functions (PDFs) of the calculated particle aerodynamic diameter for urban zone Z1 are shown in Figure 12 a and 12b. In the same way as also for preojected area diameter (d_{pa}) it was consistently found that the Inverse Gaussian (IGD), Generalized Extreme Values (GEVD), and Lognormal (LOGD) distributions were 3 best fits for particle aerodynamic size in summer and winter season.

The PDFs provide a quantitative description of the aerosol size distribution in terms of distribution parameters. For the aerodynamic diameter (d_a), the distributions yielded a mean value of 5.5851 μm with a large standard deviation of 5.4048 μm in the summer season, and a mean value of 5.0835 μm with a standard deviation of 4.1088 μm in the winter season. These values indicate the central tendency and dispersion of the aerosol size distribution for each season.

The aerodynamic diameter represents an important parameter in characterizing aerosol particles, as it influences their behavior in the atmosphere, including their settling velocity and ability to be transported over

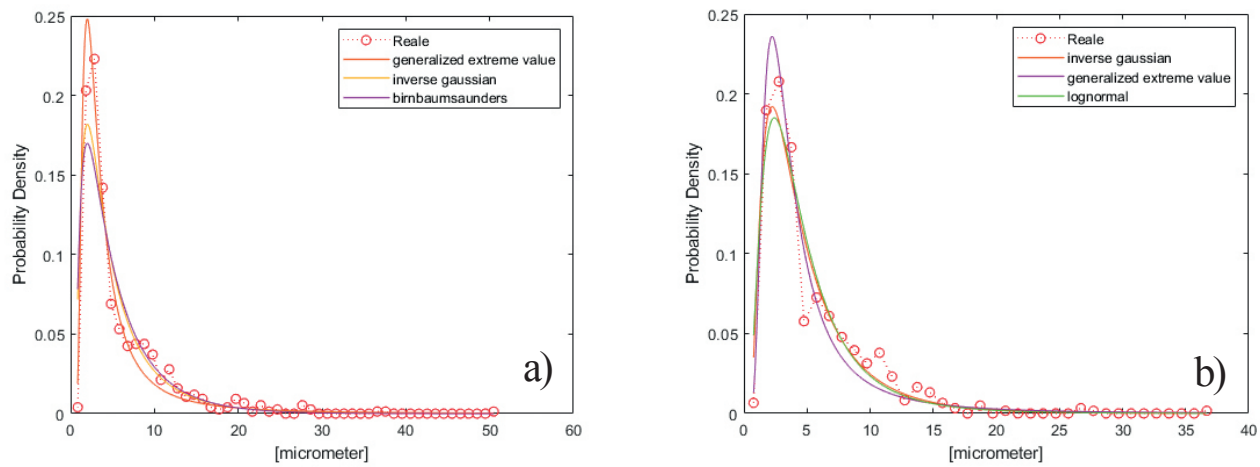

Figure 12. Probability distribution functions (PDFs) of particle aerodinamic diameter during a) summer and b) winter season.

long distances. The wide standard deviation observed in both seasons suggests a significant variability in the size distribution, indicating the presence of particles with diverse sizes. As can be seen from the distribution plots, comparing the results presented in Figure 12a and 12b with, respectively, results of the projected area diameter in Figure 7a and 7b, the aerodynamic size distribution is shifted towards the greater diameters. Particle size distribution indicates that 90% (in summer) and 85% (in winter) of particles have aerodynamic diameters less than 10 μm. This result agrees with Reid et al. (2003) findings that the size distributions determined by use of optical particle counters suggest a more varied nature and a much larger size. The present study shows that physical dimensions of irregular particles greater than 1 μm are smaller than any other equivalent dimensions. Thus, a correction function is required to be implemented in optical particle counters based on scattering measurements and aerodynamic diameter, as suggested by other studies (Reid et al., 2003; Pfeipher et al., 2016).

Particles with the same physical diameter but different densities have different aerodynamic diameters. Particles with greater density (mineral particles having an average diameter of 2.52 g cm^{-3}) have an aerodynamic diameter greater than the particles with a lower density (carbon particles and sea salt particles with a density of about 1 g cm^{-3} and 1.3 g cm^{-3}, respectively). Another aspect of the difference between the measured physical diameter and the aerodynamic diameter is particle shape. Particles with the same density may have different shapes. This is typical for aluminosilicate particles containing Si, Al, and Fe, but having different shapes, spherical or irregular ones (Cvetkovic et al., 2012; Morantes et al., 2021). Also, biogenic particles composed of carbon can be rounded (pollens), ellipsoidal (spores), or irregular (insect or plant fragments). Correction factor (Huningham factor) affects aerodynamic diameter values of particles with a physical diameter greater than 1μm.

Aerosol particle classification

Based on their morphology and chemical composition 4118 aerosol particles were categorized. Natural particles consisted mostly of soil dust (minerals) and biogenic (biological fragments, spores, fungi, etc) particles. Soil dust particles were shaped irregularly with rough surfaces and sometimes as agglomerates, while biogenic particles were highly structured, with rounded shapes and smooth surfaces. Anthropogenic particles emitted from combustion processes were predominantly spherical and rounded with a smooth surface. This type of particle was found not only as individual particles, but mostly in the fine mode as aggregates with carbon matrix known as soots. Table 3 gives a summary of particle classes and their corresponding abundance and elemental composition for examined samples. The abundance of particles is represented by the percentage of particle number over the total number of analysed particles.

The most abundant particles were classified into main groups such as Alumino -silicates (fly ash and soil particles), Ca-rich, carbonaceous (soot and biological particles), Si-rich, Fe-rich, sea salt and mixed particles.

The physical diameter of spherical fly ash particles produced by combustion ranged from 1 μm to 5 μm. Soot particles originated from combustion, especially from vehicle emissions occurring in chain-like or cluster aggregates (Fruhstorfer and Niessner, 1994; Bhandari et al., 2019) were found with diameters in the range of 0.5-2 μm. Particles originating from biomass burning with diameters from 2 to 5 μm contributed a small amount to total particle volume.

Irregularly shaped mineral particles of soil aluminosilicates and Ca-rich particles were distributed over a total size range of 0.5 μm to 28 μm, with a predominance in the 1-6 μm fraction. Si-rich mineral particles were found in coarse fractions. They have a layered structure and irregular and elongated shapes. Spherical particles rich in Fe produced by high melting temperatures in the metallurgical industry have not been detected in any of the samples. Detected Fe-rich particles in the analysed samples have irregular shapes with diameters in the middle and coarse fractions. Fresh sea salt particles have a regular and typical structure with diameters from 2 to 4 μm. Whereas aged sea salt particles undergoing chemical transformations and change of sizes and shapes in the atmosphere, were mostly found in medium mode from 1 to 2 μm. Mixed particles were found commonly rounded with a diameter smaller than 3 μm. Our results agree with the conclusion by Okada et al. (2001), Mogo et al. (2005), Xie et al. (2005), Iordanidis et al. (2007), Lu et al. (2007), Shen et al. (2007), Perez et al. (2008), Cvetkovic et al. (2012), Pachauri et al. (2013), Bora et al. (2021) and Morantes et al. (2021).

Urban site Z1

875 and 742 individual particles, respectively in summer and winter season are analysed based on elemental composition and morphological characteristics obtained by SEM/EDS and ImageJ software. Results for urban site Z1 show that small number of super coarse particles were observed, while no particles larger than 28 μm were observed. Aluminosilicate soil particles, Ca-rich and biogenic particles are the only particles identified in the super coarse mode. The dominant particles are aluminosilicates and calcium-rich particles. Aluminosilicates comprise 31% of summer and 37% of the total analysed particles in winter. Fly ash particles

account for 46.5% and 44.5% of aluminosilicate particles in summer and winter, respectively. Because the sampling point is located alongside the main boulevard, the results of fly ash particles remain highly affected by traffic. Season variation for soot particles is not very significant. Dispersion effects are more favorable during the summer season. The results for spherical fly ash particles found almost equally in summer and winter suggest a common source, mainly from vehicle emissions. Another source is the waste incineration area, a hotspot in the northwestern part of the city, not far from the main boulevard. The strong east and northeast winds that dominate the city of Vlora perform a kind of natural protection of the city against this hotspot.

Soot particles constitute 13.3%, and 18.1% of the total analysed particles in summer and winter, respectively. They are mainly found in fine and medium modes. A difference is observed in the summer and winter seasons. Fine, medium, and coarse mode account for 72.41%, 18.1%, and 9.48% in summer and 47%, 35%, and 19% in winter, respectively, suggesting that their source is different. As most of the soot particles in summer are typically from high-temperature combustion, traffic is the leading source in summer. During the winter, more soot particles from wood biomass burning were observed than in summer, with larger dimension characteristics. The primary source of soot particles in winter remains traffic, but there is also an additional contribution from wood burning. Wood burning is not the primary heat source of the city, and other local activities contribute such as restaurants, pizzerias near the sampling point, or the transportation of soot particles from the other areas of the city by winds.

All mineral particles (aluminosilicate soil particles, Ca, Si, Fe, and mixed particles) make up the dominant part of the total particles, 46% in summer and 53% in winter. Aluminosilicate soil particles make up 16.6% and 20.4%, while Ca-rich particles make up 17.8% and 22.6% of the total analysed particles in winter and summer, respectively. Aluminosilicate particles are related to the anthropogenic processes of combustion at low temperatures. Ca-rich particles dominate coarse mode, especially in winter, and originate mainly from soils, construction activities, and road dust raised by traffic and winds. The increase of mineral particles during winter is explained by the effects of erosion and numerous pollutants added by unmaintained infrastructure and the influence of Mediterranean air masses. During the sampling period, the lungomare project of the city was being carried out and the inert materials caused high pollution of soil particles. Due to this high presence of soil particles and strong winds, the dust is dispersed almost throughout the city, and the dispersion effects are unfavorable. Mineral particles found in analysed samples contained traces of toxic metals such as Fe, Cu, Ni, Cr, Er, and Sc are linked to traffic-related sources (Armiento et al, 2013; Zeb et al., 2018; Bora et al., 2021). Highest percentage of them was found in the fraction of fine particles, and their irregular shape makes them potentially respirable by the respiratory system.

Fresh sea salt particles dominate the particles of this type and constitute 17.3% and 9.7% of the total in summer and winter. Lower temperatures, higher humidity, and precipitation cause a marked decrease in these particles in winter. The observed sea salt particles range in diameter from 1-4 μm. No traces of toxic metals were found in these particles, and they do not pose a health risk. Also, the square shape and average diameter greater than 2 μm do not make them potentially breathable.

Biogenic particles account for 9% and 2.7% of total particles in summer and winter. Dominated biogenic particles were found in the coarse mode. No biogenic particles were observed in the fine fraction. The dominant biogenic particles found were fragments of plants or insects. Spore and mold particles were found in a tiny percentage due to the favorable ventilation conditions of the city. The city lacks parks, and the main boulevard has no vegetation besides palm trees, so no significant seasonal change was expected in this area. They are transported in the summer by winds from the rest of the city, which is greener.

Particles classified as mixed were mainly found in medium (43% and 44%), fine (40% and 28%), and coarse modes (16% and 28%) in winter and summer, respectively. Seasonal variation of medium mode is insignificant, while it is much more pronounced in coarse and fine fashion. In the summer season, fine particles dominate, which can be more related to the effects of traffic. In winter, the coarse mode dominated, which are related to soil materials and their mixing with vehicle emissions. These particles contained moderate amounts of toxic metals such as Ti, Cu, Fe, Mn, etc. They pose a health risk not only from their content but also from their high amount of sharpening and relatively small dimensions (they have an average diameter smaller than 2 μm). Particles with variable amounts of Al, Mg, Si, Ca, Fe, and Sc are also soil particles from the surrounding hills' rocks. Ti, S-rich particles observed in both seasons probably come from the abrasion of vehicle wheels. Particles rich in Cu and S were observed in samples collected during the summer are coming from the north where copper ores are found or probably transported by continental air masses.

Urban site Z2

The analysis of 286 particles at the Z2 site yielded the following results, as presented in Table 3: 14.0% of the

particles were spherical fly ash particles (aluminosilicates) in the size range of 0.5-5 µm. These particles are commonly associated with combustion processes, such as the burning of fossil fuels or biomass. 16.4% of the particles were irregular soil particles (aluminosilicates) in the size range of 0.5-24 µm. These particles are likely derived from local soil sources and can be generated through natural processes or human activities. 19.2% of the particles were composed of calcite (Ca-rich) in the size range of 0.5-28 µm. Calcite is a mineral primarily made up of calcium carbonate and can originate from various sources, including geological formations and anthropogenic activities. The samples exhibited an enhanced contribution of sea salt and silica particles, which can be attributed to aerosols originating from the sea surface and coastal areas rich in sand. Pure silica particles, characterized by high amounts of silicon (Si) and oxygen (O), can occur naturally as well as be produced artificially through various industrial processes. Iron (Fe)-rich particles accounted for 5.2% of the total particles at this site, suggesting a higher abundance compared to the Z1 site. This indicates the presence of local sources, and it is plausible that activities at the nearby port, including emissions from diesel exhausts and the presence of corroded ship parts, along with aerosol transport by western winds, contribute to these particles.

The proximity of the sampling site to a busy traffic road suggests that vehicle emissions may be the source of 13.3% of soot particles and 14% of fly ash particles. Mineral particles from construction materials, crust, soil dust, and resuspended road dust are the main sources of mineral particles at this site. The elevated concentrations of silicon (Si), aluminum (Al), calcium (Ca), iron (Fe), sodium (Na), manganese (Mn), magnesium (Mg), chromium (Cr), cadmium (Cd), sulfur (S), and phosphorus (P) indicate their presence in these particles.

These results indicate a complex mixture of aerosol particles at the Z2 site, with contributions from various sources such as combustion processes, local soil sources, sea salt and silica particles, industrial activities, and vehicular emissions.

Suburban site Z3

The results show that mineral particles (aluminosilicate soils, Ca particles, Fe particles, and Si particles) constitute the central part of 42% of the total analysed particles in summer and 55% in winter in the site Z3. This seasonal change in the relative abudance of mineral particles is due to erosion, building demolitions and added soils in the city, and the dumping of inert materials mainly near this area. Soot particles account for 7.5% and 13.1% in summer and winter, respectively. Fly ash particles account for 12.5% of summer and 8% of winter. These results indicate that their sources are different. Mostly the soot particles observed in both seasons are typical of low-temperature combustion processes, but soot aggregates typical of high-temperature fuel combustion are also present in the samples. There is heavy traffic in summer than in winter in this area. Dominant westerly winds during daylight hours bring traffic discharges to the monitoring point. From the daily cycles of fine particles an increase in fine particles during the night hours was reported (Miço et al., 2019a). The main source of fly ash and soot particles in this area is the open waste burning in the evening hours in the city landfill, which is located on the northeast side of the monitoring point. The predominance of northeasterly winds during the night affects the transport of particles from this area.

During the summer, there is a higher percentage of fly ash particles because this area is influenced by increased traffic. The first two sampling days in summer were on the weekend, so the fly ash particles were more abundant. Another source of fly ash particles and soot particles is their transportation from the rest of the city due to the predominance of northeasterly winds. The presence of the trees makes the distribution of particles, even in the coarse fraction, more complex. Si-rich particles constitute a high percentage due to the sandy character of the area and the effects of erosion.

During the summer, it was observed that the individual particles that dominate alongside the soil particles are the sea salt particles (18.6%). The formation of sea salt particles is favored by high temperatures and their dispersion by winds blowing from the west. It is observed that the sea salt particles have a smaller percentage on days with greater humidity. Biogenic particles (mainly plant fragments) account for about 12% in summer and 9.1% in winter, reflecting the greening effect almost the same in both measurement periods.

Background site Z4

Results for the site Z4 which is located 350 m above sea level show that fly ash particles make up 4.5%, and soot particles make up 4.1% of the total particles. In this period, there is a predominance of marine air masses, and the local air masses that bring anthropogenic particles of fly ash and soot from the city are not favored.

Mineral particles make up 56% of the total particles, aluminosilicates make up about 19%, and calcium-rich particles make up 24.7%. Sea salt particles make up 17.2%, while particles of biological nature (plant and animal residue, spores, and pollen) consisted of minor P, Cl and S contents make up about 12%.

Urban site Z5

The results from the Z5 site, where three samples were collected at the second floor of a residential building

located in the north part of the city, are presented in Table 3. The findings indicate the following:

Soil particles accounted for 24% of the total particles, making them the most abundant particles at this site. These soil particles are likely derived from the surrounding environment, including nearby hills, soil aggregates, and unpaved roads. Calcite particles represented 25% of the total particles. Calcite is a mineral composed of calcium carbonate and can be sourced from geological formations or anthropogenic activities. Fly ash particles accounted for 10.7% of the analysed particles. Fly ash is a byproduct of combustion processes, typically associated with the burning of fossil fuels in power plants or industrial activities.

Soot particles comprised 12.3% of the total particles. These particles are produced during incomplete combustion of fuels and biomass and often have a chain-like morphology. The high traffic density of trucks and vans in the roadside sampling site suggests that traffic emissions are a significant source of these soot particles. The presence of very irregular particles indicates a diverse mixture of aerosols at this site, potentially originating from various sources such as soil, road dust, and combustion processes.

Biogenic particles, likely originating from vegetation, constituted 5.8% of the total particles. The low percentage suggests that this area lacks vegetation, which may be due to factors such as poor maintenance or environmental conditions.

Overall, the dominant sources of particles at the Z5 site appear to be traffic emissions, soil and road dust, as well as the poor maintenance of the area. The high concentration of road dust, resuspended multiple times and mixed with vehicle emissions, can contribute to the observed particle composition and concentrations in this location.

Urban site Z6

Sampling site was selected at the second floor of children's hospital building. Measurements were carried out over 24-h period of 6 days starting on 12 January 2015. The aerosol particle pollution is expected to be high due to heavy diesel trucks and because the building is in a traffic trap, without any obstacles, trees, or other buildings. This road is very narrow and closed on both sides forming a corridor, rarely cleaned and washed. Fly ash particles were dominated by fine mode. These particles, although spherical, are considered hazardous to health due to the content of toxic metals and are easily respirable for very small sizes. Even the soot particles are dominated by fine mode. These results suggest that the source of fly ash and soot particles is common. The percentage of fly ash particles examined was 17.4% of the total analysed particles and 49% of the aluminosilicate group particles. Soot particles account for 19.4% of the total particles, the highest amount observed from all areas, higher even than on the main boulevard. Typical anthropogenic fly ash and soot particles make up about 36% of the analysed particles. The number of fly ash and soot particles detected was almost the same on different days. Since examined fly ash and soot particles were typical particles of high-temperature combustion, their common source is traffic-related. Mineral particles make up about 46%, mixed particles about 6%, and the rest from biogenic particles (4%) and sea salt particles (8%). Aluminosilicate and calcium particles have approximate abundance. The higher abundance of mineral particles analysed in the fine mode can be explained by creating a stable suspension of fine dust from the road soils, re-raised by the traffic. The irregular shape and the content of traces of toxic metals that are characteristic of mineral particles, re-raised several times and mixed with vehicle exhausts, make them hazardous to health.

Rural site Z7

In the rural area, where sampling was carried out in February 2015, fly ash particles account for 5.2%, and soot particles about 7.5%, indicating an area free from vehicle emissions. In this area, the particles rich in calcium have the maximum relative amount of all the areas taken in the study, 33.5%. Ca-rich particles found were dominant in the fine particle fraction. The primary source is the presence of a gravel pit processing inert materials near the sampling point, plus the effects of soil erosion and other soils. Mineral particles (Al/Si, Ca, Si, and Fe) make up 60% of the total particles.

Source identification of urban aerosol particles

The results of the relative abundance for each group of particles regarding all analysed sites in the city of Vlora, summarized for the summer and winter seasons are shown in Figure 13a and 13b, respectively. Mineral particles from the soil dominate both seasons, increasing about 27% in winter. For winter, there is also an increase in soot and fly ash particles by 40%. Sea salt particles have a high percentage in summer and a lower percentage in winter, decreasing by about 94%. Biogenic particles in winter decrease about 2.3 times. The other particles, Si and Fe, remain almost unchanged in both seasons.

The primary sources of aerosol particles are the direct emissions of vehicles and waste burning, mineral soils, road dust raised by winds or induced by traffic, construction-related anthropogenic activities, air masses that transport aerosol particles from further distances, biomass, and sea salt. The processes of pollutant dispersion are complex. Vlora has the bay of the sea to the west and the hills to the east. Pollutants emitted during

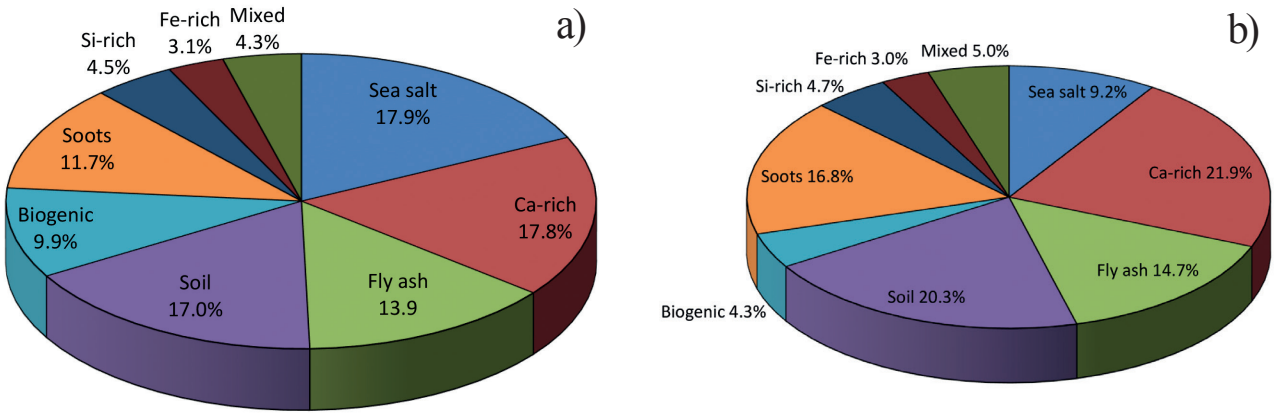

Figure 13. Aerosol particle characterisarion in urban atmosphere during a) summer and b) winter season.

the day can penetrate the city's interior via westerly sea winds until they meet the hill barrier. During the night, the northeast winds transport the pollutants toward the sea. Stable conditions over the sea, due to the presence of the peninsula, prevent the spread of pollutants, and during the day, the pollutants return to the city through sea winds, causing persistent presence of pollutants in the urban atmosphere in Vlora. The influence of local air masses coming from the country's north is confirmed by the presence of round Cu-rich particles found in two analysed samples. During the winter season, in addition to local anthropogenic pollutants, meteorological conditions such as higher relative humidity and lower mixing height (boundary layer height), usually 500-1000 m, favor the accumulation of pollutants, causing aerosol particles to remain for a longer time in the atmosphere. This study shows that in urban areas, various local sources, such as vehicle exhausts, waste burning, and road dust, are the dominant sources of aerosol particles in the urban atmosphere. To reduce concentrations of aerosol particles in the urban atmosphere in addition to lower traffic, one of the most effective ways would be to reduce dust emissions through road maintenance and timely cleaning of inert materials. The highest particle concentrations were observed in samples collected when the air masses were local and when the air masses came from the Mediterranean and the Sahara.

CONCLUSIONS

Analysis of individual aerosol particles were performed using SEM/EDS and image processing techniques to investigate the relations between the morphology, size, composition, and origin of aerosol particles. Photomicrographs of scanning electron microscope were processed to calculate equivalent diameters and shape factors for aerosol particles. Based on particle morphological characteristics and their chemical composition, nine groups of aerosol particles were determined: aluminosilicates (fly ash and soil particles), Ca-rich particles, carbon particles (soot particles and biogenic particles), sea salt particles, Si-rich particles, Fe -rich particles, and other particles (or mixed). Based on shape factors particles are classified as: elongated and irregular-shaped, regular triangular, regular square, pentagonal, ellipsoidal, hexagonal, octal- to decagonal particle, rounded and not perfectly spherical and perfectly spherical.

The process of fitting theoretical distributions to the observed aerosol data can provide insights into the physical and chemical processes associated with the aerosol particles. In this study, several theoretical distributions were examined, and based on the goodness of fit, the generalized extreme values, inverse Gaussian, and lognormal distributions consistently resulted as the best fitted functions among the five best fits. The choice of these specific probability density functions suggests that the aerosol particles exhibit characteristics that are well represented by these distributions. The generalized extreme values distribution, for example, is often used to model extreme events or rare occurrences, indicating that the aerosol particles may exhibit occasional extreme values or behaviors. The inverse Gaussian distribution, on the other hand, can describe a range of processes, including particle growth, aggregation, or transformation. Its selection as one of the best fitted distributions suggests that such processes may be relevant in explaining the observed aerosol data. The lognormal distribution, a commonly observed distribution for aerosol particles, is often associated with single source aerosols. Its presence among the best fitted distributions indicates that certain aerosol components may follow lognormal behavior, potentially linked to specific sources or formation

mechanisms.

Overall, the selection of these probability density functions highlights the heterogeneity and complexity of the aerosol system under investigation. The fitting features observed in the study reflect the diverse physical and chemical processes that influence the aerosol particle population, emphasizing the need for a comprehensive understanding of these processes to accurately describe and model aerosol behavior.

Investigated aerosol particles were distributed relatively over a wide range from 0.5 μm to 28 μm fitted.

By accounting for volume equivalent and diameter aerodynamic shape factor, this study develops the method to calculate the aerodynamic diameter. Aerodynamic diameter of particles greater than 1 μm was found to be greater than physical or projected area diameters. Particles with greater density (mineral particles) have an aerodynamic diameter greater than those with lower density (carbon particles and sea salt particles). Fly ash and soil particles with the same density but different shapes have different aerodynamic factors. The same occurs for carbonaceous particles. Our results confirmed the shape correction must be made for particle size measurement instruments. Biogenic particles, which can be rounded (pollens), ellipsoidal (spores), or irregular (insect or plant fragments), have different aerodynamic diameters. The surface of the most of analysed particles is rough with sharpened edges that support the fine particle deposition process with a possibility of evolving chemical reactions after the particle formation process increasing the health hazard of aerosol particles.

No significant seasonal variation of total aerosol particles was observed due to the invariability of particle deposition flux on the filter when the metric is particle number. The main contribution of fine aerosol particles arises from combustion particles smaller than 0.5 μm, which were excluded in this study. However, elevated concentrations for summer coarse particles were observed. Windblown and traffic-induced dust (composed of aluminosilicates, ca-rich, and mineral particles), sea salt particles, and biogenic particles are the three main groups that contributed differently during the two seasons. Traffic flow effects increased during summer and were balanced by windblown dust. The increase in coarse particle concentrations during the summer is primarily due to the extras of sea salt and biogenic particles. The influence of hygroscopic growth of particles in the winter season due to the humidity was not considered during the SEM analysis. The presence of traces of heavy metals in most of the analysed particles indicates the contamination of soil particles, given that for a long time these dusts are present in the urban atmosphere, being re-raised several times and mixed with the direct emissions of vehicles.

Data on morphological characteristics and chemical composition taken from microscopy techniques, variations in time and space of aerosol particles, meteorological conditions and trajectories of air masses can be used integrated to identify potential sources of aerosol particles in the atmosphere.

ACKNOWLEDGEMENTS

The authors thanks Department of Chemistry, University of Ioannina for the facilities of SEM Lab offered. Also appreciate Professor Philipos J. Pomonis and Dr. Eleni Tsaousi for SEM-EDS analysis of aerosol samples and their useful suggestions.

We would also like to thank the reviewers whose valuable comments and very helpful suggestions improved the quality of our paper.

REFERENCES

Abramoff M.D., Magalhaes P.J., Ram S.J., 2004. Image Processing with ImageJ. Biophotonics International 11(7), 36-42.

Allen T., 2003. Powder Sampling and Particle Size Determination, Elsevier Science; 1 edition.

Andersson A., 2021. Mechanisms for log normal concentration distributions in the environment. Scientific Reports 11, 16418 https://doi.org/10.1038/s41598-021-96010-6.

Armiento G., Inglesis M., Taglioni M.S., Montreali R.M., Nardi E., Palleschi S., Piga L., Sacco F., Leopoldo S., Gianfagna A., 2013. A comprehensive approach to the investigation of particulate PM2.5: preliminary results. Periodico di Mineralogia 82, 199-216. doi: 10.2451/2013PM0012.

Baron A.P. and Willeke K., 2001. Aerosol measurement: Principles, Techniques, and Applications, 2nd Ed. John Wiley and Sons, Incterscience Publictaions.

Barthelmy D., 2006. Mineralogy Database, /http://www.webmineral.com.

Bell M.L. and Davis D.L., 2001. Reassessment of the Lethal London Fog of 1952: Novel indicators of acute and chronic consequences of acute exposure to air pollution. Environmental Health Perspectives 109 (Supp. 3), 389-394.

Bhandari J., China S., Chandrakar K.K., Kinney G., Cantrell W., Shaw R.A., Mazzoleni L.R., Girotto G., Sharma N., et al. 2019. Extensive Soot Compaction by Cloud Processing from Laboratory and Field Observations. Scientific Reports 14; 9, 11824. doi: 10.1038/s41598-019-48143-y.

Bora J., Deka P., Bhuyan P., Sarma K.P., Hoque R.R. 2021. Morphology and mineralogy of ambient particulate matter over mid-Brahmaputra Valley: Application of SEM-EDX, XRD, and FTIR techniques. SN Applied Sciences 3, 137.

Brostrøm A., Kling K.I., Hougaard K.S., Mølhave K., 2020. Complex Aerosol Characterization by Scanning Electron Microscopy Coupled with Energy Dispersive X-ray Spectroscopy. Scientific Reports 10, 9150.

Carabali G., Mamani-Paco R., Castro T., Peralta O., Herrera

E., Trujillo B., 2012. Optical properties, morphology, and elemental composition of atmospheric particles at T1 supersite on MILAGRO campaign. Atmospheric Chemistry and Physics 12, 2747-2755.

Cvetkovic Z., Logar M., Rosic A., Civic A., 2012. Mineral composition of the airborne particles in the coal dust and fly ash of the Colubara basin (Serbia). Periodico di Mineralogia 81, 205-223.

Dhoqina P., Miço S., Alushllari M., 2019. Fractal dimension of soot aggregates, AIP Conference Proceedings, 10th Jubilee International Conference of the Balkan Physical Union - Sofia, Bulgaria (26-30 August 2018), 2075, 130022.

Dimitriou K., Tsagkaraki M., Zarmpas P., Mihalopoulos N., 2022. Impact of spatial and vertical distribution of air masses on PM10 chemical components at the Eastern Mediterranean-A seasonal approach. Atmospheric Research 266, 105974.

Dockery D.W., Pope C.A., Xu X., Spengler J.D., Ware J.H., Fay M.E., Ferris B.G., Speizer F.E., 1993. An association between air pollution and mortality in six US cities. The New England Journal of Medicine 329, 1753-1759.

Draxler R.R. and Rolph G.D., 2003. HYSPLIT (Hybrid Single-Particle Lagrangian Integrated Trajectory) Model Access via the NOAA ARL READY Website (http://www.arl.noaa.gov/ready/hysplit4.html).

Dunbar C.A. and Hickey A.J., 2000. Evaluation of probability density functions to approximate particle size distributions of representative pharmaceutical aerosols. Journal of Aerosol Science 31, 813-831.

Ebert M., Hof M.I., Weinbruch S., 2002. Environmental scanning electron microscopy as a new technique to determine the hygroscopic behavior of individual aerosol particles. Atmospheric Environment 36, 5909-5919.

EN 12341, Ambient air - Standard gravimetric measurement method for the determination of the PM10 or PM2,5 mass concentration of suspended particulate matter.

EN 14907:2005, Ambient air quality - Standard gravimetric measurement method for the determination of the PM2,5 mass fraction of suspended particulate matter.

EPA, 2002. Guidelines for the application of SEM/EDX analytical techniques to particulate matter samples, EPA 600/R-02/070.

Ferreira P.J., Rasteiro M.G., Figuereido M.M., 1993. Influence of shape in particle image analysis. Particulate Science and Technology 11, 199-206.

Fruhstorfer P. and Niessner R., 1994. Identification and classification of airborne soot particles using an automated SEM/EDX. Microchimica Acta 113, 239-250.

Hassan M. and Lau R., 2009. Effect of particle shape on dry particle inhalation: study of floWability, aerosolization, and deposition properties. AAPS PharmSciTech 10, 1252-1262.

Heyder J., Gebhart J., Rudolf G., Schiller C.F., Stahlhofen W., 1986. Deposition of particles in the human respiratory tract in the size range 0.005-155 mm. Journal of Aerosol Science 17, 811-825.

Hinds W.C., 1999. Aerosols technology: properties, behavior, and measurements of airborne particles, 2nd Ed., J. Wiley and Sons, N.Y.

Horvath H., 1998. Influence of Atmospheric Aerosols upon the Global Radiation Balance, in Atmospheric Particles, vol. 5, edited by R.M. Harrison and R.E. van Grieken, pp. 543-596, Wiley-InterScience, New York.

Isik H. and Cabalar A.F., 2022. A shape parameter for soil particles using a computational method. Arabian Journal of Geosciences 15, 581.

Iordanidis A., Buckman J., Triantafyllou A.G., and Asvesta A.I., 2007. Atlas of airborne particles from Kozani area, Northern Greece, Bulletin of the Geological Society of Greece, vol. XXXX, Proceedings of the 11th International Congress, Athens, May 2007.

Kaaden N., Massling A., Schladitz A., Muller T., Kandler K., Schutz L., et al., 2009. State of mixing, shape factor, number size distribution, and hygroscopic growth of the Saharan anthropogenic and mineral dust aerosol at Tinfou, Morocco. Tellus 61B, 51-63.

Kandler K., Lieke K., Benker N., Emmel C., Kupper M., Mullerebert D., Ebert M., Scheuvens D., Schladitz A., Schutz L., Weinbruch S., 2011, Electron microscopy of particles collected at Praia, Cape Verde, during the Saharan Mineral Dust Experiment: particle chemistry, shape, mixing state and complex refractive index. Tellus B, Chemical and Physical Meteorology 63, 475-496.

Kandler K., Schutz L., Deutscher C., Ebert M., Hofmann H., Jackel S., Jaenicke R., et al., 2009. Size distribution, mass concentration, chemical and mineralogical composition and derived optical parameters of the boundary layer aerosol at Tinfou, Morocco, during SAMUM 2006. Tellus B, Chemical and Physical Meteorology 61, 32-50.

Kómar L., Wallner S., Kocifaj M., 2022. The significant impact of shape deviations of atmospheric aerosols on light monitoring networks. Monthly Notices of the Royal Astronomical Society, Volume 512, Issue 2, May 2022, Pages 1805-1813, https://doi.org/10.1093/mnras/stac548.

Le Thi-Cuc and Tsai Chuen-Jinn, 2021. Inertial Impaction Technique for the Classification of Particulate Matters and Nanoparticles: A Review. KONA Powder and Particle Journal, doi: 10.14356/kona.2021004.

Li W., Liu L., Xu L., Zhang J., Yuan Q., Ding X., Hu W., Fu P., Zhang D., 2020. Overview of primary biological aerosol particles from a Chinese boreal forest: Insight into morphology, size, and mixing state at microscopic scale. Science of The Total Environment 719, 137520, doi: 10.1016/j.scitotenv.2020.13752.

Lu S.L., Shao L.Y., Wu M.H., Jiao Z., Chen X.H., 2007. Chemical elements and their source apportionment of PM10 in Beijing urban atmosphere. Environmental Monitoring and Assessment 133, 79-85.

Lu C.E., Newbury D.E., Goldstein J.I., Williams D.B., Romig A.D., Armstrong J.T., Echlin P., Fiori C.E., Joy D.C., Lifshin E., Peters K., 1990. Scanning Electron Microscopy, X-ray Microanalysis, and Analytical Electron Microscopy-A Laboratory Workbook 36.

Masuda H., Higashitani K., Yoshid H.K., 2012. Powder Technology Handbook, CRC Press, 3 Edition, 33-47.

Miço S., Tsaousi E., Deda A., Pomonis. P., 2015. Characterization of airborne particles and source identification using SEM/EDS, ECB; 4, 224-229.

Miço S., Alushllari M., Deda A., Dhoqina P., Tsaousi E., 2019a. The variability of aerosol particle number concentrations using optical particle counter and scanning electron microscope, AIP Conference Proceedings, 2075, 160037.

Miço S., Deda A., Tsaousi E., Alushllari M., Pomonis P., 2019b. Complex refractive index of aerosol samples. AIP Conference Proceedings, AIP Publishing Women in Physics: Birmingham, UK, 2017060002.

Mogo S., Cachorro V.E., De Frutos A.M., 2005. Morphological, chemical and optical absorbing characterization of aerosols in the urban atmosphere of Valladolid. Atmospheric Chemistry and Physics 5, 2739-2748.

Morantes G., González J.C., Rincón G., 2021. Characterisation of particulate matter and identification of emission sources in Greater Caracas, Venezuela. Air Quality, Atmosphere and Health 14, 1989-2014.

Mushtaq Z., Sharma M., Bangotra P. et al., 2022. Atmospheric Aerosols: Some Highlights and Highlighters, Past to Recent Years. Aerosol Science and Engineering 6, 135-145.

Nafiseh S.N. and Jason S.O., 2019. Calibration of optical particle counters with an aerodynamic aerosol classifier, Journal of Aerosol Science 138, 105452, ISSN 0021-8502.

Okada K., Jost H., Kenji K., Yu Q., 2001. Shape of atmospheric mineral particles collected in three Chinese arid-regions. Geophysical Research Letters 28, 3123-3126.

Olson E., 2011. Particle shape factors and their use in image analysis-Part 1: Theory, J. GXP Compliance, Peer Review 15(3), 85-96.

Pachauri T., Singla V., Satsangi Aparna, Lakhani A., Maharaj Kumari K., 2013. SEM-EDX Characterization of Individual Coarse Particles in Agra, India, Aerosol and Air Quality Research 13, 523-536.

Papayannis A., Balis D., Amiridis V., Chourdakis G., Tsaknakis G., Zerefos C., Castanho ADA., Nickovic S., Kazadzis S., Grabowski J., 2005. Measurements of Saharan dust aerosols over the Eastern Mediterranean using elastic backscatter-Raman lidar, spectrophotometric and satellite observations in the frame of the EARLINET project. Atmospheric Chemistry and Physics 5, 2065-2079.

Perez N., Pey J., Querol X., Alastuey A., Lopez J.M., Viana M., 2008. Partitioning of major and trace components in PM10-PM2.5-PM1 at an urban site in Southern Europe, Atmospheric Environment 42, 1677-1691.

Peters A., Wichmann H.E., Tuch T., Heinrich J., Heyder J., 1997. Respiratory Effects are Associated with the Number of Ultrafine Particles. American Journal of Respiratory and Critical Care Medicine 155, 1376-1383.

Pfeifer S., Müller T., Weinhold K., Zikova N., Martins dos Santos, S., Marinoni, A., Bischof, O.F., Kykal, C., et al., 2016. Intercomparison of 15 aerodynamic particle size spectrometers (APS 3321): uncertainties in particle sizing and number size distribution, Atmospheric Measurement Techniques 9, 1545-1551, https://doi.org/10.5194/amt-9-1545-2016.

Piazzola J., Bruch W., Desnues C., Parent P., Yohia C., Canepa E., 2021. Influence of Meteorological Conditions and Aerosol Properties on the COVID-19 Contamination of the Population in Coastal and Continental Areas in France: Study of Offshore and Onshore Winds. Atmosphere 12, 523. https://doi.org/10.3390/atmos12040523.

Pope C.A., Dockery D.W., Schwartz J., 1995. Review of Epidemiological Evidence of Health Effects of Particulate Air Pollution, Inhalation Toxicology 7, 1-18.

Post J.E. and Buseck P.R., 1984. Characterization of individual particles in the Phoenix urban aerosol using electron beam instruments. Environmental Science & Technology18, 35- 42.

Querol X., Pey J., Pandolfi M., Alastuey A., Cusack M., Pérez N., Moreno Kallos G., Kleanthous S., 2009. African dust contributions to mean ambient PM10 mass-levels across the Mediterranean Basin, Atmospheric Environment 43, 4266-4277.

Reid J.S., Jeffrey S.R., Halflidi H.J., Hal B.M., Alexander S., Dennis L.S., Steven S.C. et al., 2003. Comparison of size and morphological measurements of coarse mode dust particles from Africa. Journal of Geophysical Research 108, 8593,

Reid E.A., Reid J.S., Meier M.M., Dunlap M.R., Cliff S.S. and co-authors, 2003. Characterization of African dust transported to Puerto Rico by individual particle and size segregated bulk analysis. Journal of Geophysical Research 108, 7.1-7.22.

Romano S., Perrone M.R., Becagli S., Pietrogrande M.C., Russo M., Caricato R., Lionetto M.G., 2020, Ecotoxicity, genotoxicity, and oxidative potential tests of atmospheric PM10 particles, Atmospheric Environment 221, 117085.

Salvador P., Pey J., Pérez N. Querol X. and Artinano B., 2022. Increasing atmospheric dust transport towards the western Mediterranean over 1948-2020. npj Climate and Atmospheric Science 5, 34. https://doi.org/10.1038/s41612-022-00256-4.

Schraufnagel D.E., 2020. The health effects of ultrafine particles. Experimental and Molecular Medicine 52, 311-317.

Seinfeld J.H. and Pandis S.N., 1998. Atmospheric Chemistry and Physics, from Air Pollution to Climate Change, 1326 pp., Wiley-InterScience, New York.

Seo J., Park D. -S.R., Kim J.Y., Youn D., Lim Y.B., Kim Y., 2018. Effects of meteorology and emissions on urban air quality: a quantitative statistical approach to long-term records (1999-2016) in Seoul, South Korea. Atmospheric Chemistry and Physics 18, 16121-16137.

Shandilya K.K. and Kumar A., 2010. Morphology of single inhalable particle inside public transit biodiesel fueled bus. Journal of Environmental Sciences 22, 263-270,

Shen Z.X., Cao, J.J., Arimoto R., Zhang R.J., Jie D.M., Liu S.X., Zhu C.S., 2007. Chemical Composition and Source Characterization of Spring Aerosol over Horqin Sand Land in Northeastern China. Journal of Geophysical Research 112, D14315. Perez et al 2008, Xie et al., 2005.

Sielicki P., Janik H., Guzman A., Namiesnik J., 2011. The progress in electron microscopy studies of particulate matters to be used as a standard monitoring method for air dust pollution, Critical Reviews in Analytical Chemistry 41, 314-334.

Sokolik N.I. and Toon B.O., 1999. Incorporation of mineralogical composition into models of the radiative properties of mineral aerosol from UV to IR wavelengths, Journal of Geophysical Research 104, No. D8, 9423-9444.

Tan Z., 2014. Properties of Aerosol Particles. In: Air Pollution and Greenhouse Gases. Green Energy and Technology. Springer, Singapore. https://doi.org/10.1007/978-981-287-212-8_4.

Tian J., Liu E., Jiang L., Jiang X., Sun Y., Xu R., 2018. Influence of particle shape on the microstructure evolution and the mechanical properties of granular materials, Comptes Rendus Mécanique 346, 460-476,

Taunton E.A., Gunter E.M., Nolan P.R., Phillips I.J., 2011. Characterization of minerals in pleural plaques from lung tissue of nonhuman primates. Periodico di Mineralogia 80, 167-179.

Tegen I., Lacis A.A., Fung I., 1996. The influence on climate forcing of mineral aerosol from disturbed soils. Nature 380, 419-422.

Tegen I. and Fung I., 1994. Modeling of mineral dust transport in the atmosphere: Sources, transport, and optical thickness. Journal of Geophysical Research 99, 22897-22914. doi: 10.1029/94JD01928.

U.S. EPA, 1986. Review of the National Ambient Air Quality Standards for Particulate Matter, Updated Assessment of Scientific and Technical Information, Addendum to the 1982 OAQPS Staff Paper, Report Number EPA 450/05 86-012, Strategies and Air Standards Div., Ofc. of Air Quality Planning and standards, US EPA, Research Triangle Park, NC.

Usman F., Zeb B., Alam K., Huang Z., Shah A., Ahmad I., Ullah S., 2022. In-Depth analysis of physicochemical properties of particulate matter (PM10, PM2.5 and PM1) and its characterization through FTIR, XRD and SEM-EDX techniques in the foothills of the Hindu Kush Region of Northern Pakistan. Atmosphere 13, 124.

Wu Zh. and Colbeck I., 1996. Studies of the dynamic shape factor of aerosol agglomerates. Europhysics Letters 33, 719.

West J.J., Cohen A., Dentener F., Brunekreef B., Zhu T., Armstrong B., Bell M.L., Brauer M., Carmichael G., Costa D. L., 2016. What We Breathe Impacts Our Health: Improving Understanding of the Link between Air Pollution and Health. Environmental Science & Technology 50, 4895-4904.

WHO (World Health Organization), 2006. WHO Air quality guidelines for particulate matter, oarea, nitrogen dioxide and sulphur dioxide, Global update 2005.

Xie R.K., Seipa H.M., Leinumb J.R., Winjec T., Xiao J.S., 2005. Chemical characterization of individual particles (PM10) from ambient air in Guiyang City, China, Science of the Total Environment 343, 261- 272.

Xu L., Liu L., Zhang J., Zhang Y., Ren Y., Wang X., Li W., 2017. Morphology, Composition, and Mixing State of Individual Aerosol Particles in Northeast China during Wintertime. Atmosphere 8(3), 47. https://doi.org/10.3390/atmos8030047.

Yang S.H., Jaein I.J., Rokjin J.P., Minjoong J.K., 2020. Impact of Meteorological Changes on Particulate Matter and Aerosol Optical Depth in Seoul during the Months of June over Recent Decades. Atmosphere 11, 1282.

Zeb B., Alam K., Sorooshian A., Blaschke T., Ahmad I., Shahid I., 2018. On the Morphology and Composition of Particulate Matter in an Urban Environment. Aerosol and Air Quality Research 28;18, 1431-1447.